

Chapter 4

Geoacoustic Observations on Drifting Balloon-Borne Sensors



Daniel Bowman, Jonathan Lees, James Cutts, Attila Komjathy, Eliot Young, Kayla Seiffert, Mark Boslough and Stephen Arrowsmith

Abstract Infrasound microphones on free flying balloons experience very little wind noise, can cross regions that lack ground station coverage, and may capture signals that seldom reach the Earth's surface. Despite the promise of this technique, until recently very few studies had been performed on balloon-borne acoustic sensors. We summarize the history of free flying infrasound stations from the late 1940s to 2014 and report on results from a series of studies spanning 2014–2016. These include the first efforts to record infrasound in the stratosphere in half a century, the presence of a persistent ocean microbarom peak that is not always visible on the ground, and the detection of distant ground explosions. We discuss the unique operational aspects of deploying infrasound sensors on free flying balloons, the types of signals detected at altitude, and the changes to sensor response with height. Finally, we outline the applications of free flying infrasound sensing systems, including treaty verification, bolide detection, upper atmosphere monitoring, and seismoacoustic exploration of the planet Venus.

D. Bowman (✉) · M. Boslough · S. Arrowsmith
Sandia National Laboratories, Albuquerque, NM, USA
e-mail: dbowma@sandia.gov

J. Lees
Department of Geological Sciences, University of North Carolina,
Chapel Hill, NC, USA

J. Cutts · A. Komjathy
Jet Propulsion Laboratory, California Institute of Technology,
Pasadena, CA, USA

E. Young
Southwest Research Institute, San Antonio, TX, USA

K. Seiffert
Department of Geological Sciences, University of North Carolina,
Chapel Hill, NC, USA

4.1 Introduction

Geoacoustic sensor networks are almost always located on the Earth's surface (Marty 2019). There are compelling reasons, on the other hand, for fielding such networks in the free atmosphere. For example, motivations for free floating airborne acoustic stations include

- Dramatically reduced wind noise (Raspet et al. 2019)
- Placement in elevated ducts containing signals that do not reach the ground
- Greater range for direct acoustic arrivals
- Three-dimensional acoustic wave field above the ground is virtually unexplored
- The acoustic energy flux from the lower to the upper atmosphere has never been measured directly

Naturally, there are many technological and conceptual challenges to fielding sensors in the atmosphere. Constant atmospheric motion makes station keeping difficult, whereas powered flight systems, on the other hand, may introduce unacceptable noise levels. The temperature, solar radiation, and pressure environments as elevation rises can become increasingly hostile to delicate instrumentation. Most seismo-acoustic signal processing techniques assume a stationary receiver, virtually unattainable above the surface of the Earth. Deploying fixed aperture sensor arrays is very difficult because a rigid structure of the necessary size is prohibitively difficult to launch. Multiple separate units will continuously change their orientation with respect to each other and eventually drift apart.

These possibilities and challenges motivated a return to balloon-borne stations after a hiatus of over half a century. The series of experiments began as a proof of concept and evolved into the first operationally robust-free flying geoacoustic sensor networks since the advent of the digital era. This chapter describes the history, operational aspects, experimental results, and recent applications of free flying balloon-borne geoacoustic stations.

4.2 History

The first attempt to record acoustic waves above the Earth's surface began in the aftermath of World War II. After the discovery of the Sound Fixing and Ranging channel (SOFAR; Officer 1958) in the ocean, investigations commenced into a possible atmospheric analogue. The project, called MOGUL, began in 1946. Its objective was to detect the acoustic signature of Soviet nuclear blasts and ballistic missile flights at extreme range using balloon-borne microphones. Although the project only lasted about 4 years, it led to significant improvements in balloon technology. However, there is no information on the acoustic signals detected during the flights. Project MOGUL's enduring legacy is the Roswell Incident, in which one of the balloons landed in eastern New Mexico and was mistaken for a UFO (Weaver and McAndrew 1995; Peebles 1997).

Another series of balloon flights in the early 1960s investigated acoustic waves between 0.2 and 150 Hz at altitudes up to 22 km. Over 30 flights were conducted. Some of these deployments consisted of one microphone hanging tens of meters beneath another one, allowing for direction of arrival estimation (Wescott 1964a; Coffman 1965).

The main finding of this experiment was that background noise in the 17–22 km altitude range consists of acoustic radiation from atmospheric turbulence (Wescott 1961, 1964a, b; Meecham and Wescott 1965). Time delays between channels on double sensor flights indicated that the waves originated from a planar region of randomly distributed acoustic sources below the balloons. Wescott (1964a) further observed a 30 dB background noise variation between day and night.

Spectrograms revealed signatures of piston engine aircraft above about 30 Hz (see Fig. 4.1). Doppler shifts and ground-reflected modes were both observed. Pulses of broadband signal were related to jet aircraft. Other, unknown events were recorded as well. These events were below 5 Hz and had amplitudes in the 1 Pa range. They occurred several times per hour in the summer and once every 1–2 h in the winter. They lasted from one minute to several minutes.

The next half century saw very few attempts to record geoacoustic signals above the surface of the Earth. Microphones on dropsondes were used to capture blast waves from underground and surface explosions (Banister and Hereford 1991) and sensors on tethered aerostats were employed to quantify sonic booms from experimental aircraft (Veggeberg 2012; Naka et al. 2013). Research into free flying geoacoustic arrays began again in 2014 and is presently ongoing; results from this work comprise the remainder of the chapter.

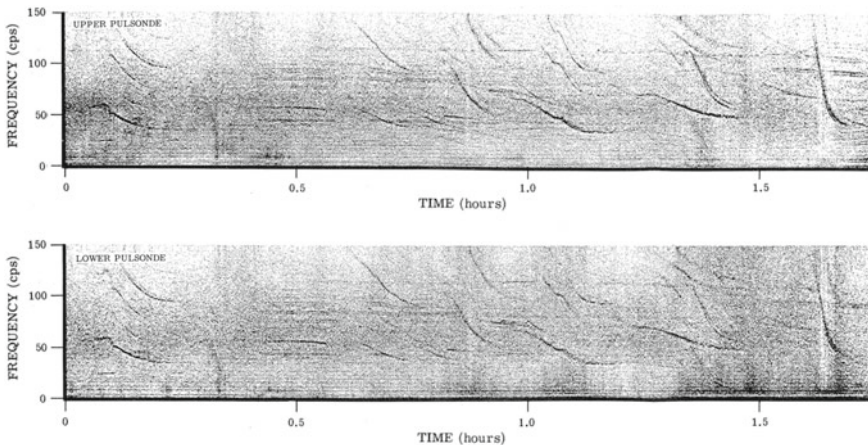


Fig. 4.1 Spectrograms from a double-sensor balloon flight on February 28, 1961 presented in Wescott (1964a)

4.2.1 Recent Progress

4.2.1.1 The HASP 2014 and 2015

Geoacoustic research in the stratosphere recommenced in 2014 as part of the High Altitude Student Platform (HASP). The HASP is an annual zero pressure balloon flight from Ft. Sumner, New Mexico, that carries up to 12 student payloads into the stratosphere for 5–29 h depending on atmospheric conditions (Guzik et al. 2008). Geoacoustic payloads were deployed on the 2014, 2015, and 2016 flights (Fig. 4.2). Instrumentation on the HASP 2014 consisted of a single Omnirecs Datacube digitizer, located on the gondola, with three InfraBSU microphones strung out on the “flight ladder” connecting the gondola to the parachute. The successful operation of the sensors and digitizer during the flight provided strong indication that geoacoustic data acquisition was possible at high altitudes. Initial results indicated that the stratosphere contained a highly unusual infrasound wave field (Bowman and Lees 2015a), but evidence from later experiments suggested that these signals were most likely from non-acoustic sources.

The HASP 2015 flight lasted much longer (about 29 h) due to low-wind speeds in the stratosphere. Two Omnirecs Datacube digitizers and six InfraBSU microphones

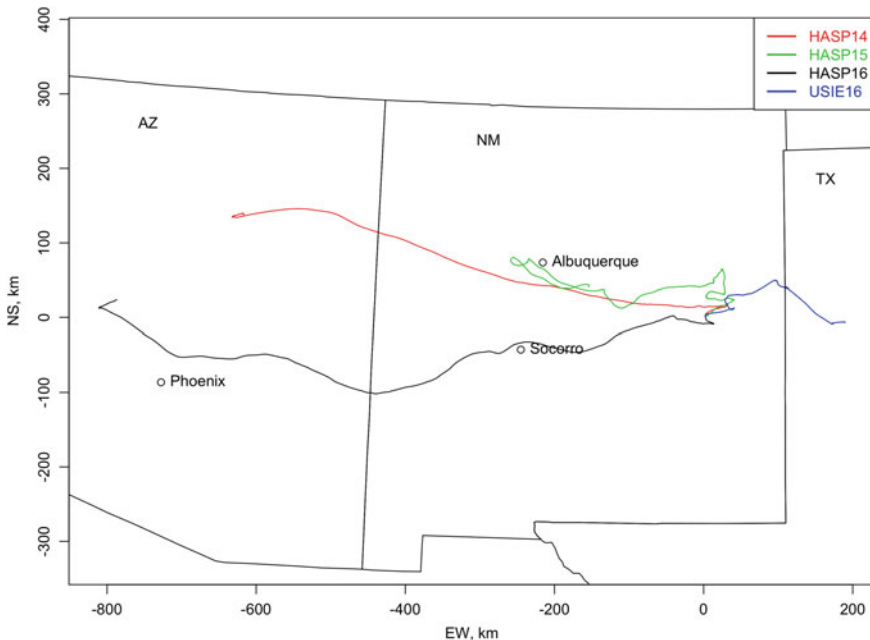


Fig. 4.2 Flight paths of the HASP and SISE/USIE balloon flights

were deployed, five on the flight ladder and one on the gondola. Two Gem infrasound sensor/loggers developed by Boise State University (see Anderson et al. 2018) were also on board. A spectral peak in the ocean microbarom range was identified during the quietest period of the flight (Bowman and Lees 2016). However, results from the HASP 2015 showed, again, severe interference from non-acoustic sources, which led to identification of this interference on the HASP 2014 as well (Bowman 2016).

4.2.1.2 The 2015 Weather Balloon Flight

Concerns about electronic interference experienced by the HASP 2014 and 2015 experiments prompted a new sensor/digitizer design that eschewed long analog signal cables, introduced a mechanically disabled “control” microphone, and implemented a microphone pair with reversed pressure polarities. This sensor trio was designed to rigorously distinguish between true pressure fluctuations and spurious signals. They were flown to an altitude of 28 km on a continuously ascending latex weather balloon over central North Carolina in Fall 2015. The design worked as expected. It also recorded the burst of the weather balloon at the top of its trajectory and confirmed a drop in wind noise amplitude at certain elevations as had been seen on the first two HASP flights. The three-component microphone configuration pioneered during this flight directly led to the successes of three flights in 2016.

4.2.1.3 The HASP 2016

The HASP 2016 was designed to distinguish between pressure signals and those induced by other phenomena. Two independent payloads were flown, each configured using the design tested on the weather balloon as described above. One consisted of an Omnirecs Datacube with three InfraBSU infrasound microphones contained in a small box on the gondola, and the other consisted of a Trimble Ref Tek 130 digitizer with three InfraBSU microphones and a triple-axis accelerometer located in a box attached to the flight ladder. The suspicious signals recorded on the first two HASP flights were absent, and a prominent ocean microbarom peak was present through most of the flight. Thus, the HASP 2016 successfully demonstrated the operation of a reliable geoacoustic sensor network in the stratosphere.

4.2.1.4 SISE/USIE

Previous experiments lacked “ground truth” acoustic sources with which to evaluate the detection thresholds of balloon-borne geoacoustic sensors. Thus, an active source experiment was fielded during Fall 2016. The Stratospheric Infrasound Sensitivity Experiment (SISE) (Young et al. 2016) and the UNC-Sandia Infrasound Experiment (USIE) were included as secondary payloads aboard a Columbia Scientific Ballooning Facility zero-pressure flight out of Ft. Sumner, New Mexico (Fig. 4.2). The SISE

payload was mounted on a boom extending from the gondola. It consisted of ten differential pressure transducers, five of which contained mechanical filters similar to those used in InfraBSU microphones. Data were digitized using a custom board. The USIE payload was located beneath the flight deck of the gondola. It consisted of two Omnirecs Datacube digitizers, five InfraBSU microphones (one control, two with normal polarity, two with reversed polarity), and a Chaparral 60 microphone. See Sect. 4.5.1 for an explanation of “control” microphones and the polarity reversal method. In addition, a prototype solar hot air balloon carrying a lightweight Gem infrasound acquisition system (Anderson et al. 2018) was launched about an hour after the zero pressure balloon. An extensive network of ground geoaoustic stations was deployed in the expected flight path of the zero pressure balloon and near the blast site.

On the day of the flight, three 3000 lb ANFO detonations (2400 lb TNT equivalent) were carried out at the Energetic Materials Research and Testing Center (EMRTC) in Socorro, New Mexico. One shot was performed at 1800 UTC, the second at 2000 UTC, and the third at 2230 UTC. All three shots were detected by instrumentation on the zero pressure balloon, and the second was detected by the Gem on the solar hot air balloon. The solar hot air balloon was over 250 km from the blast site when it detected the second shot, and the zero pressure balloon was 395 km from the blast site when it recorded the third shot. No ground station further than 6 km from the blast site recorded the first shot, but the second two explosions were detected on a single ground station 180 km from the blast site. None of the ground stations near the zero pressure balloon’s trajectory recorded any of the blasts.

4.2.1.5 ULDB 2016

A geoaoustics sensor package was included as a secondary payload on the NASA Ultra Long Duration Balloon (ULDB) flight launched from Wanaka, New Zealand on May 16, 2016. The package contained an Omnirecs Datacube digitizer with three infraBSU microphones: one control and reversed polarity pair. The ULDB landed in Peru on July 2, 2016 for a total flight duration of 46 days, including one circumnavigation of the South Pole (Fig. 4.3). The sensor package recorded data for 17 days, starting at about 5 min prior to launch. This time period included one circumnavigation of Antarctica. The data set returned by this experiment is the longest continuous acoustic recording in the stratosphere thus far. The ocean microbarom was present continuously, and other signals of unknown provenance were detected from time to time. The constant microbarom peak suggests that free flying microphones may be more consistently sensitive to far-field infrasound in this frequency range than stations on the Earth’s surface. This is because local noise often obscures the ocean microbarom peak, particularly during the day (Bowman et al. 2005).

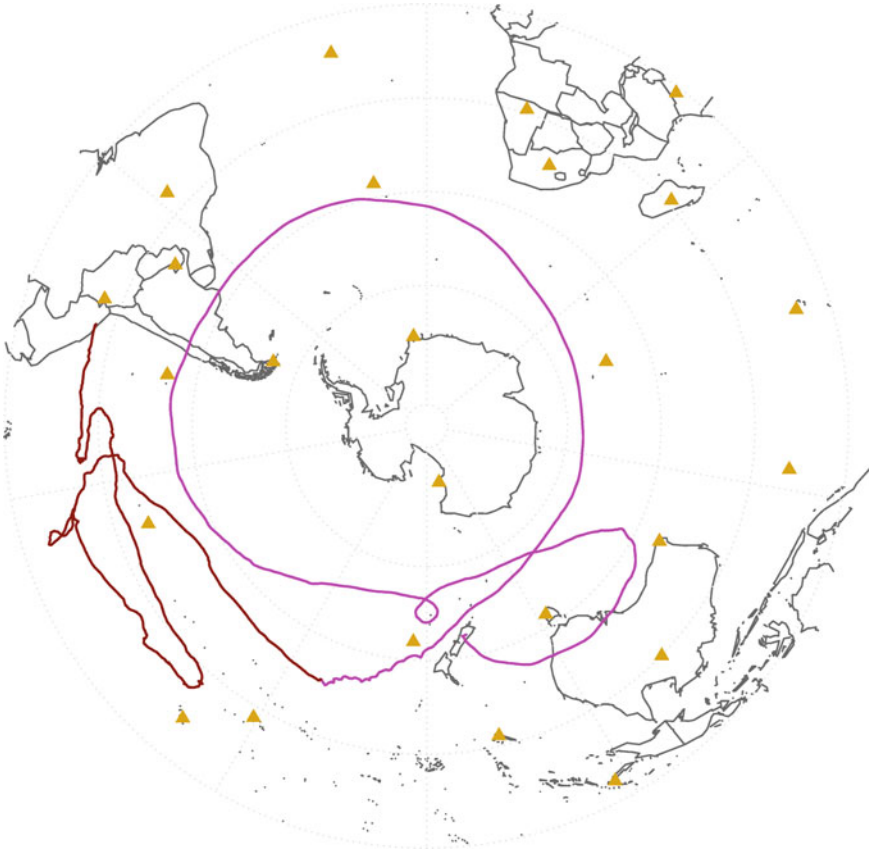


Fig. 4.3 Flight path of the 2016 ULDB experiment. The magenta line shows when the sensor package was operational. The red line shows the path of the balloon after the sensor ran out of battery power. The triangles denote International Monitoring System infrasound stations

4.3 Operational Aspects of Free Flying Sensors

4.3.1 Flight Systems

Balloons can drift at altitudes ranging from <1 km (Doerenbecher et al. 2016) to over 53 km (Saito 2014). Flight durations can range from a few hours to 744 days (Lally 1991). Balloon designs vary depending on altitude, flight duration, launch facilities, and cost. Since 2014, infrasound sensors have been launched on continuously ascending weather balloons, zero pressure balloons, superpressure balloons, and solar hot air balloons (see Figs. 4.4 and 4.5).



Fig. 4.4 A zero pressure balloon (left) and a solar hot air balloon (right) launched during the SISE/USIE infrasound experiment

- Weather balloons consist of an elastic envelope that expands as the balloon rises. Eventually, the balloon bursts, and the payload parachutes back down to Earth. These flights are seldom more than 3 h long and reach altitudes of 28–40 km.
- Zero pressure balloons consist of rigid envelopes with vents. When the balloon reaches its neutral buoyancy, or “float” point, excess gas is vented to prevent pressurization of the envelope. These balloons can fly for several days, but must drop ballast during the night to maintain flight. Therefore, time aloft is limited by the amount of ballast on board.
- Superpressure balloons are unvented, retaining their lift gas through the day/night cycle and eliminating the need for ballast. They can fly for over 2 years (Lally 1991). For additional details on the performance and dynamics of zero-pressure and superpressure balloons, see Yajima et al. (2009) and Morris (1975).
- Solar-powered hot air balloons utilize a dark-colored envelope to absorb sunlight, heating the air inside the envelope enough to gain positive lift (Bowman et al. 2015). They fly as long as the sun shines and land after sunset.

See Fig. 4.6 for time/altitude plots of infrasound payloads on the balloon types described above.

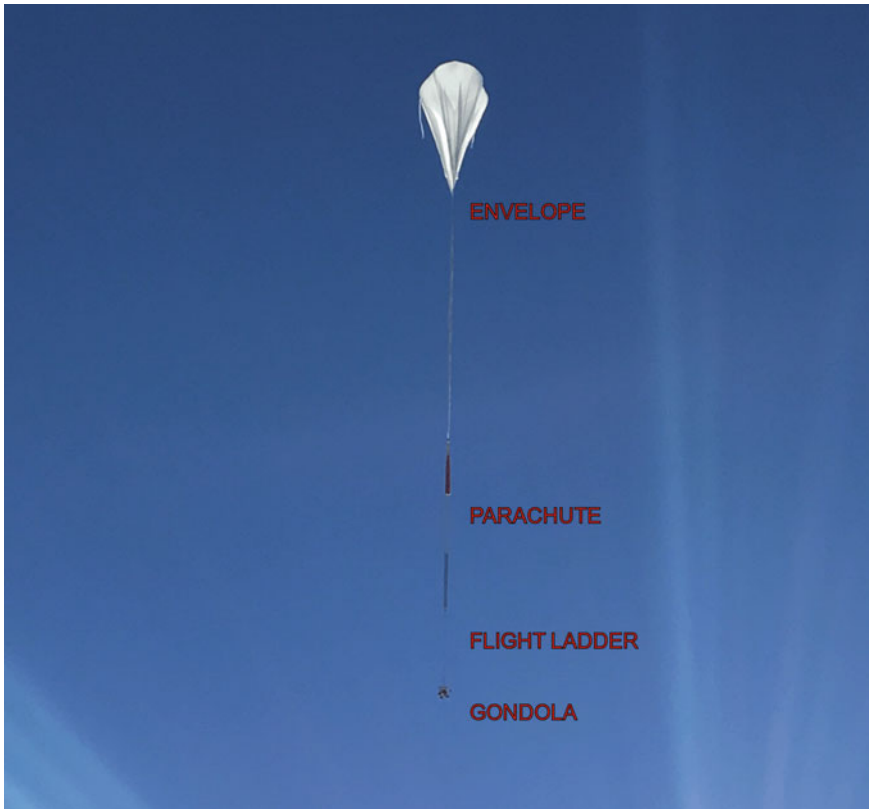


Fig. 4.5 The SISE/USIE zero pressure balloon several minutes after launch. Instrumentation on the HASP flights was located on the gondola and attached to the flight ladder, whereas microphones on SISE/USIE and the ULDB were located on or in the gondola. The distance from the gondola to the top of the balloon is approximately 150 m

4.3.2 *Environmental Considerations*

Geoacoustic sensors on balloons experience very different pressure and temperature conditions than those on the surface. They can experience high levels of interference from other instrumentation on the balloon (tracking and telemetry systems, other payloads) and possibly the ambient environment as well (cosmic rays). This can affect survivability of instrumentation at altitude, maintenance of appropriate signal-to-noise ratios, and the ability to distinguish between acoustic waves and spurious phenomena.

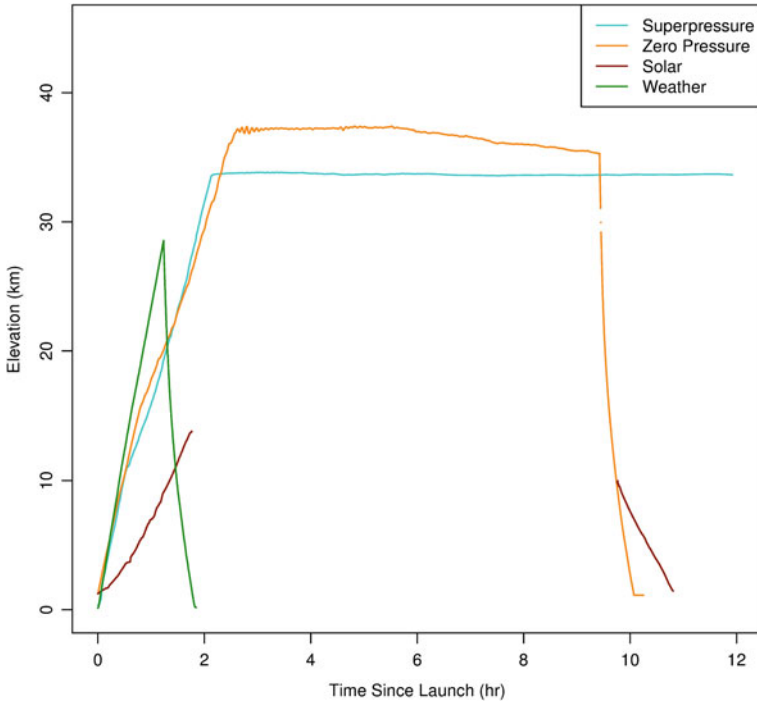


Fig. 4.6 Elevation profiles for four different types of balloons recently used in geoacoustic studies. The superpressure balloon example is from the first few hours of the 2016 ULDB flight. The zero pressure and solar hot air balloons are from the 2016 SISE/USIE experiment. Note that the solar hot air balloon lost GPS tracking above 13.8 km. The weather balloon trajectory is from the test flight in 2015

4.3.2.1 Pressure and Temperature

Ambient pressure decreases by over two orders of magnitude from sea level to the middle stratosphere. This changes the thermal resilience of instrumentation, affects the frequency response of infrasound sensors, and impacts the absolute pressure amplitude of acoustic waves. As air density decreases, thermal transfer changes from convection dominated to radiation dominated. As a consequence, the actual air temperature is much less significant than objects' albedo and exposure to sunlight. Dark-colored objects heat up dramatically during the day, whereas temperatures after sunset plummet to levels seldom achieved on the Earth's surface. For example, a black square exposed to sunlight reached over 84 °C during the HASP 2014 flight. At night on the HASP 2015, flight ladder instrumentation dropped to -55 °C. Furthermore, instrumentation that relies on air flow for cooling may become dangerously warm. Thus, it is important to perform pre-flight thermal/vacuum testing to ensure instrumentation can survive extreme temperatures and low pressures. For example, all HASP payloads must operate nominally during a 6–8 h test in which temperature is

varied from -40 to $+40$ Celsius at surface and stratospheric pressures before being allowed to fly.

Microphones are extremely sensitive to minute pressure fluctuations by design. Their calibrations may be invalid in the low-pressure environment at altitude. Also, they can be damaged by the rapid pressure drop during ascent or the even more rapid pressure rise during descent. All recent experiments have utilized vented backing volume microphones for this reason. This allows the sensors to equilibrate once they reach the float portion of the flight, although they are often saturated during ascent and descent.

A vented backing volume microphone has one chamber open to ambient pressure and another chamber connected to the atmosphere by a capillary tube. The chamber/capillary tube combination creates the acoustic equivalent of a resistor–capacitor circuit, allowing long period pressure fluctuations through but blocking high-frequency ones. A diaphragm between the open and partially blocked chamber deflects in response to unequal pressures between the two, creating a voltage that is then digitized. The result is a mechanical high-pass filter (Marcillo et al. 2012; Mutschlechner and Whitaker 1997). The corner period of this filter is

$$T = 2\pi RC \quad (4.1)$$

where R is the acoustic resistance of the capillary tube and C is the acoustic capacitance of the backing chamber.

Assuming Poiseuille flow, the acoustic resistance is

$$R = \frac{8\eta}{\pi r^4} l \quad (4.2)$$

where η is the shear viscosity of the fluid, r is the radius of the capillary tube, and l is the length of the capillary tube (Mutschlechner and Whitaker 1997).

The acoustic capacitance of the backing chamber is

$$C = \frac{V}{\gamma \bar{P}} \quad (4.3)$$

where V is the backing volume, γ is the adiabatic gas constant, and \bar{P} is ambient pressure. Since acoustic capacitance is inversely proportional to ambient pressure, microphones on high-altitude balloon flights often have orders of magnitude greater corner periods than the same microphone design at sea level (see Fig. 4.7). Acoustic resistance is somewhat sensitive to temperature due to variations in shear viscosity, but is relatively insensitive to pressure changes (Ames Research Staff 1953). Thus, the capacitance term dominates corner frequency variations with altitude. Sensor frequency response may vary with decreasing air density due to the upward shift in the isothermal/adiabatic transition, but the effect is likely small and will not affect the corner period (see Mentik and Evers 2011, Sect. 4). However, a sensor characterization study in a pressure chamber capable of reproducing stratospheric conditions

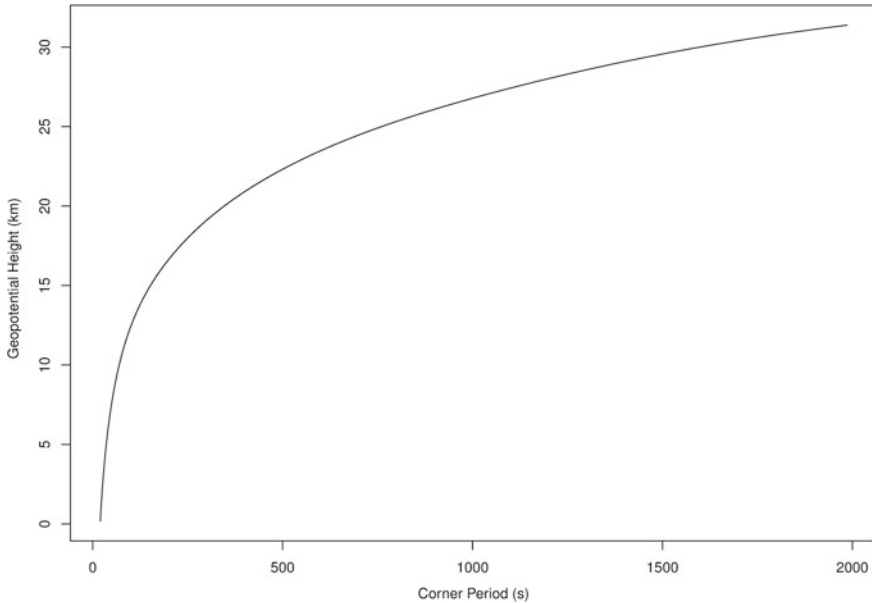


Fig. 4.7 Model of the frequency response of a vented infrasound microphone with altitude. The microphone has a 20 s corner period at 1000 mb. The pressure/height profile is from the August 9, 2014 18Z analysis Global Forecast System model run over Chapel Hill, North Carolina. This figure originally appeared in Bowman (2016)

would be valuable. An initial attempt is reported in Bowman (2016), but the experiment would have benefited from a better controlled acoustic source.

4.3.2.2 Signals from Non-Pressure Sources

Infrasound sensors on high-altitude balloons may acquire signals that are not related to pressure fluctuations. These include amplitude spikes and narrow band, constant frequency signals. Spikes tend to occur during the latter part of the ascent and throughout the float period. They vary with instrument position on the flight system. For example, during the SISE/USIE flight, they were present on the SISE payload, which was hanging from a boom projecting from the gondola. They were not seen on the USIE payload, which was beneath the flight deck and behind metal solar shields. They were observed on the HASP 2014 and 2015 flights, in which microphones and digitizers were relatively unshielded, but not during the HASP 2016, when all equipment was in thicker containers. The cause of these spikes is unclear, but they are probably not related to mechanical jostling or temperature variations. This is because the SISE and USIE payloads were on the same gondola, and SISE was very well insulated; yet SISE-detected spikes and USIE did not. We speculate that they may be due to cosmic rays, which increase with altitude (see Dawton and

Elliot 1953), static electric discharge, or lightning-induced electromagnetic interference (Anderson et al. 2014) in some cases.

Narrow band, constant frequency signals were observed during the latter part of the HASP 2015 flight. They were polarity reversed between a pair of consistent pressure polarity microphones, indicating that they might be related to electromagnetic interference. A sporadic 10 Hz signal was seen on the ULDB 2016 flight as well. This is in the frequency range of vibrational modes observed on other balloon missions (Barthol et al. 2011), although it could be related to electromagnetic interference like that on HASP 2015 as well.

Another, more enigmatic signal class was observed on the HASP 2014 and 2015 flights (see Fig. 4.8). They do not occur during thermal/vacuum tests or full system checkouts at ground conditions prior to launch. They are quite complex and hard to explain; indeed they led Bowman and Lees (2015a, 2016) to speculate that they were a new class of acoustic waves not seen on the Earth's surface. However, reasons for attributing them to non-pressure signals include

- No phase shift across a pair of microphones vertically separated by almost 15 m
- Only present on deployments with long analog cables between sensors and digitizers (HASP 2014 and 2015)
- Not observed in over 2 weeks of flight data in 2016 (including HASP 2016)
- Presence of other interference such as spikes and polarity reversed narrow band signals
- Installation of high-power transmitting equipment on the balloon gondola
- No known Earth surface analogue

Difficulties with this explanation include

- The narrow band signals are all below 30 Hz
- Signals have the correct pressure polarity
- Similar gliding frequency bands may be present in spectrograms shown in Wescott (1964a)
- Generation mechanism of electromagnetic interference in this frequency band is unclear
- Acoustic wave field at this altitude is poorly known

The origin of these complex, narrow band signals is difficult to determine. The HASP scientific payload contained a variety of student experiments, including electric motors and radio transmission equipment, that could have generated electromagnetic radiation. The HASP gondola telemetry system utilizes high-power transmitters as well. Interference from ground-based anthropogenic electromagnetic signals is possible, but the diagnostic 60 Hz AC power peak is not present in balloon spectra. Natural radio sources such as Schumann resonance are in the appropriate frequency range (Barr et al. 2000), but do not have the gliding characteristics shown in Fig. 4.8. The only meteorological differences between the HASP 2014 and 2015 and other New Mexico flights (the HASP 2016, SISE/USIE) was the presence of thunderstorms in the former case. This may be a clue about the cause of these signals, acoustic or otherwise. Regardless, they make detection of lower amplitude acoustic

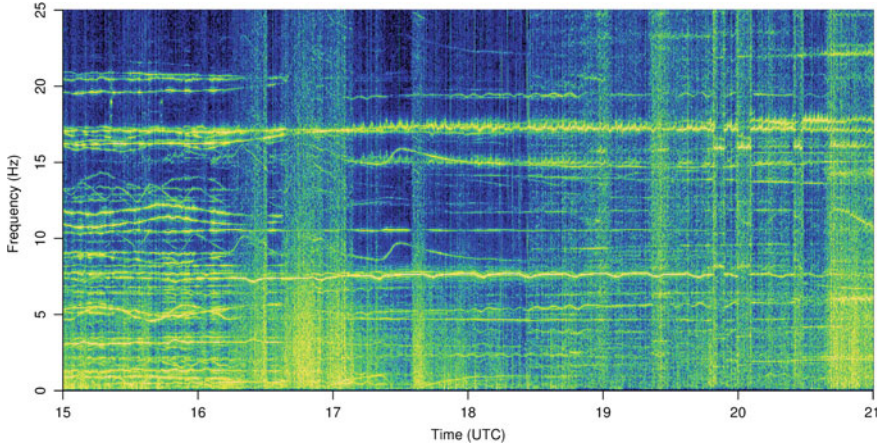


Fig. 4.8 Narrow band signals recorded during the HASP 2014 flight on August 9, 2014. Their cause is unknown

signals very difficult. Until the cause of these signals is known for certain, investigators should avoid using long analog cables during balloon infrasound deployments. If cabling is required, it should only convey digital signals and be well shielded. Alternatively, fiber optic or wireless systems could be used instead. It is also possible, albeit unlikely, that these unusual signals represent true acoustic waves that were not present on later flights.

4.3.3 Payload Design

Sensor packages designed for free flight operate under very different environmental conditions and operational restrictions than those on the ground. The need for thermal insulation must be balanced with the requirement for at least part of the package to be in direct contact with the atmosphere. The insulation material and outer covering of all equipment must be light colored or kept completely out of sunlight to prevent overheating. It is also important to prevent direct exposure to the night sky to reduce radiation loss. Despite these measures, equipment may experience extreme temperatures from time to time, and it is important that all components are able to survive such variations.

Objects on balloons can experience sudden accelerations during launch, flight termination, and landing. Thus, onboard equipment should be able to remain in place and functioning through brief periods of up to 10 g acceleration. Equipment should be protected from being crushed or shattered in case of impact on a hard surface, particularly if data are stored locally rather than telemetered. It can take days to

weeks to recover equipment if it has landed in a remote area, and water landings are possible as well.

The height ceiling of GPS chips used for timing, vibrational, and rotational modes of the flight system, and proximity to high-energy systems such as radio transmitters used for telemetry are all considerations for balloon-borne systems. Electronics on high-altitude balloons are susceptible to interference, although the source of these signals is presently unclear (recall Fig. 4.8). Thus, it is imperative to take a conservative approach. Cable length should be as short as possible, and the use of long signal wires carrying analog outputs should be strictly avoided. Shielding of the entire sensor/digitizer package using metal plates and aluminum foil appears to be an effective means of reducing spurious signals. Including a control and an opposite pressure polarity pair of microphones as described in Sect. 4.2.1.2 serves as a final sanity check.

For payloads included on large zero pressure or superpressure balloons, the entire sensor/digitizer package can be included in a hard-shelled box. Metal sides provide electronic shielding; alternatively plastic boxes can be lined with aluminum foil or plates. The exterior of the box should be painted white or covered in white tape to avoid excessive solar heating. The interior of the box should be padded with dense Styrofoam or other thermal insulation that will not off-gas at low pressures. All equipment should be securely attached to anchor points on the box. Tubes leading from microphone ports to the outside of the box can provide atmospheric coupling without sacrificing thermal control. However, it is important to make sure no object is airtight (including the box itself) to allow pressure to equalize during ascent and descent. Ideally, the instrument enclosure should be placed inside the gondola chassis to provide additional thermal control and protection against violent landings. See the left panel in Fig. 4.9 for an example.



Fig. 4.9 An infrasound payload for the HASP 2016 flight (left). Note the hard-shelled box, inner layer of insulation, and secure equipment mounting. The entire enclosure was covered in white tape before flight. The SISE/USIE solar balloon payload box (right) was constructed from the inner lining of a medical-grade foam shipper. This photo was taken during recovery of the payload and envelope several weeks after landing. The box was opened prior to taking the photo

The weight of the sensor/digitizer package is an extreme constraint when using low-lift flight systems like solar hot air balloons. In this case, reasonably robust instrumentation boxes can be constructed from medical-grade foam shipping boxes (see Fig. 4.9, right panel). These boxes are made from high-density Styrofoam that have survived 46 days in the stratosphere without noticeable off-gassing. They can be damaged upon landing, however, and thus equipment inside them should be water resistant to the extent possible.

4.4 Pressure Signals Recorded During Flight

4.4.1 *Wind Noise*

Wind noise is virtually nonexistent during the float phase of a high altitude balloon flight. This is because the flight system is a quasi-Lagrangian particle that is advected along at the mean wind velocity, resulting in exceptionally low air flow across the microphone ports (Raspet et al. 2019). Transient wind-related signals are possible even at float due to layers of turbulence (Haack et al. 2014) and the passage of gravity waves (Zhang et al. 2012), although their pressure amplitude will be several orders of magnitude lower than equivalent wind at the ground due to decreased air density at altitude. These effects may be present on existing flights although they have not been identified yet. Calculations by Bowman and Lees (2015a) indicate that vortex shedding could occur depending on the level of wind shear across the flight train, although this has not yet been seen in the data either.

Although wind noise dominates the ascent and descent, it drops rapidly with altitude. Figure 4.10 shows RMS amplitudes and a spectrogram of pressure signals recorded on infrasound microphones on a weather balloon. Wind noise is very high immediately after launch, but decreases with altitude due to progressively lower air density. A decrease in both the magnitude and variance in wind noise is observed at about 22 km altitude (just after 1 h in the spectrogram). This occurs at approximately this altitude on much larger balloons as well (the HASP, for example). The reason for this decrease may have to do with lower turbulence in the stratosphere, lower levels of wind shear, or a change in the properties of the balloon wake with decreasing Reynolds number. Results from this flight suggest that it may be possible to detect far-field acoustic signals even on an ascending balloon provided the detectors are above about 22 km. Wind mitigation strategies, such as soaker hoses like those used on ground stations, might further improve an ascending balloon's detecting capability. Methods designed to avoid the balloon's turbulent wake could be employed as well (see Barat et al. 1984).

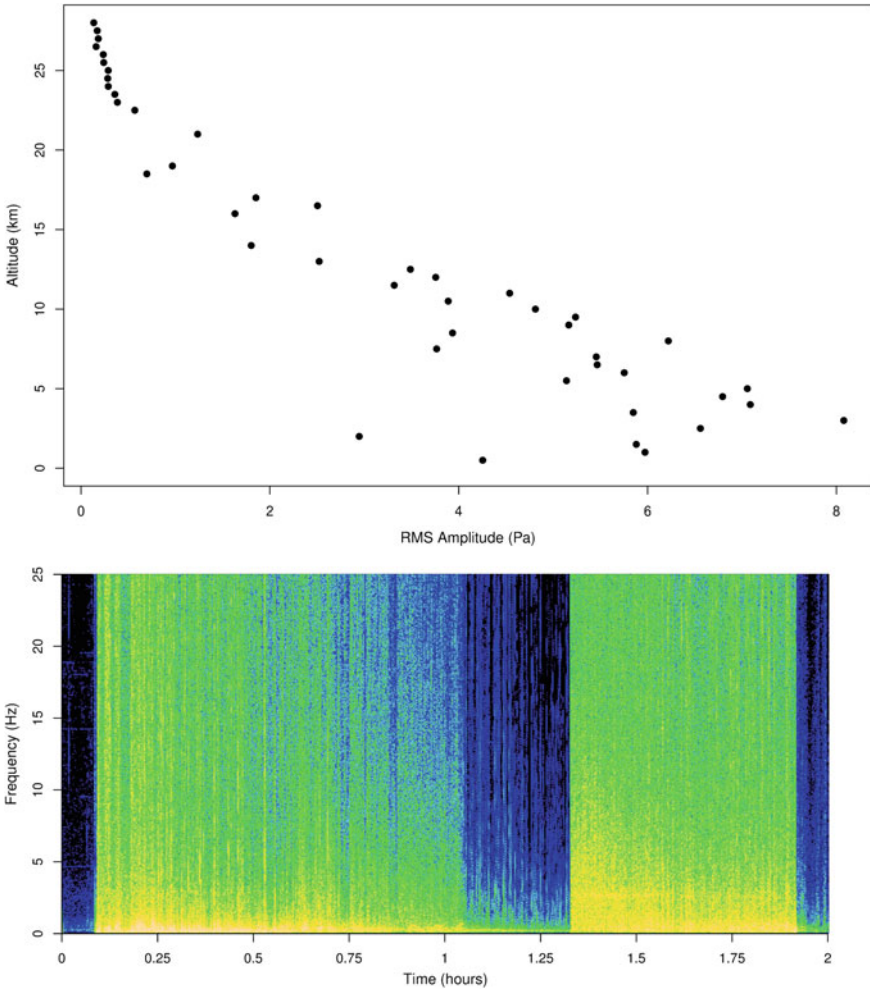


Fig. 4.10 RMS amplitude in the 0.1–20 Hz band versus elevation during ascent (top) and flight Fourier spectrogram (bottom) of pressure signals recorded on a balloon. Launch occurs at about 0.1 h after the start of the spectrogram. The balloon reaches 22 km just after the 1 h mark; this corresponds with the change in trend on the RMS amplitude plot. The balloon bursts at about 1.3 h and the payload lands just before the 2 h mark

4.4.2 Long Period Oscillations

Vertical motion of the flight system will result in pressure fluctuations. Assuming the motion is small, the signal will equal the altitude change multiplied by the local pressure gradient. Since the gradient is negative, a rise in altitude results in a drop in pressure, and vice versa. Therefore, long period pressure signals that are 180° out of phase with elevation are a diagnostic of vertical balloon motion.

The presence of a resonant peak in balloon motion spectra has been observed in several previous studies. Anderson and Taback (1991) described sinusoidal motion of an ascending zero pressure balloon, Morris (1975) discussed “overshoot” motion of zero pressure balloons upon reaching float, and Quinn and Holzworth (1987) illustrate the spectral peak of neutral buoyancy oscillations of superpressure balloons. In theory, this peak should lie just below the Brunt–Vaisälä frequency of the local atmosphere (Anderson and Taback 1991).

Pressure data from the three HASP flights as well as the USIE experiment confirm that the dominant oscillatory mode has a period of about 5 min, consistent with Brunt–Vaisälä frequencies for the middle stratosphere (Zhang et al. 2012). The highest amplitude oscillations occur just after attaining float, where they can have amplitudes of tens of Pa. The motion decays over time, but may last up to 45 min. Similar oscillations were excited during a series of ballast drops during the HASP 2015 flight, where amplitudes were under 10 Pa. Unlike the sporadic motion of the zero pressure flights described above, the superpressure and solar hot air balloons oscillated virtually continuously (Fig. 4.11). While the pressure amplitude on the superpressure balloon was below 10 Pa, the solar hot air balloon experienced up to 30 Pa excursions during the time period examined. Examination of the long period pressure power spectrum of the superpressure balloon indicated a resonant peak near the typical mid-stratosphere Brunt–Vaisälä period, as expected.

Since an object floating at neutral buoyancy behaves as a damped harmonic oscillator, energy in the resonant frequency range must be added to sustain its motion. This indicates that forcing functions, such as gravity waves, may have acted to

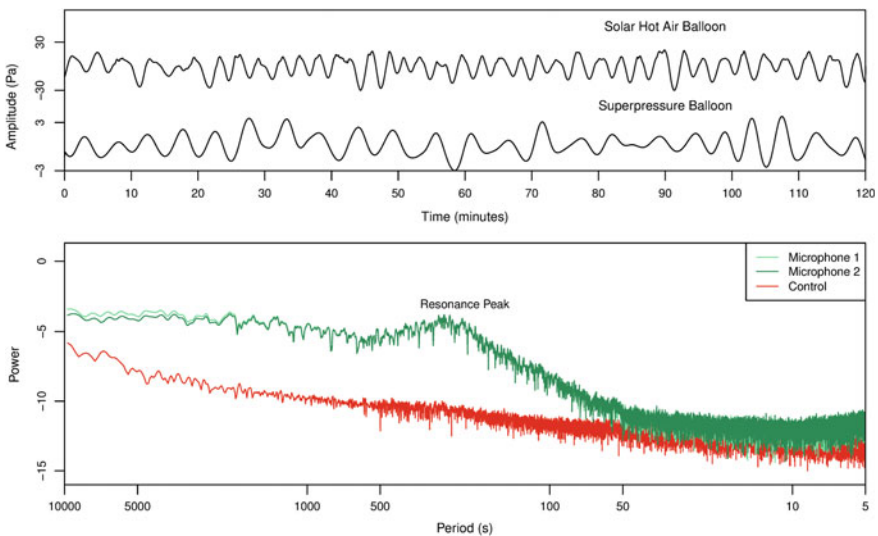


Fig. 4.11 Waveforms of long period pressure oscillations on the SISE/USIE solar hot air balloon at 15 km elevation and the 2016 ULDB superpressure balloon at 34 km. The spectra shows a 14 day Welch spectrum of long period motion on the 2016 ULDB superpressure flight

continuously excite the superpressure balloon. Since the solar hot air balloon was in a lower and more turbulent region, it may have received input from wind buffeting or even uneven heating due to envelope rotation. In this light, it is curious to note the comparatively undisturbed motion of zero pressure balloons; perhaps they are more efficiently damped or were simply not exposed to the same amount of forcing energy as the other two flights.

Pressure time series from these balloon flights have not been rigorously investigated for the presence of gravity waves, although such analysis may be promising and should be pursued in the future. However, the balloon resonant peak will obscure gravity wave characteristics in certain frequency ranges. Large pressure fluctuations have an impact on geoacoustic measurements as well: they may cause sensitive microphones to clip if their dynamic range is not sufficient. Sensors flying at stratospheric altitudes must either have a corner frequency sufficiently high enough to attenuate signals in the 100–300 second band or a dynamic range of >10 Pa.

4.4.3 *Ocean Microbarom*

The ocean microbarom is an ubiquitous infrasound signal generated by colliding surface waves in certain maritime regions (Landès et al. 2012; Waxler and Gilbert 2006; Ceranna et al. 2019). It has a frequency of 0.13–0.35 Hz and often travels great distances with minimal attenuation (Campus and Christie 2010). Microbarom detections on ground stations are strongly diurnal, with most occurring during the night. This is thought to be from lower wind noise during nocturnal hours (Bowman et al. 2005) and changes in propagation path due to semidiurnal thermospheric tides (Rind 1978). While microbaroms are often considered “noise” because they obscure signals of interest in their frequency range, they also serve as a useful reference signal to determine if infrasound sensors are operating as expected.

Spectral peaks in the microbarom range were observed on both the HASP 2014 and HASP 2015 flights (Bowman and Lees 2016), although noise in the frequency band of interest made them difficult to distinguish. However, clear ocean microbarom spectral peaks occurred on all three stratospheric flights in 2016 (ULDB 2016, HASP 2016, SISE/USIE) and on the SISE/USIE solar hot air balloon in the upper troposphere.

Figure 4.12 shows the ocean microbarom peak during the SISE/USIE experiment. The spectra were calculated over a 4.5 h period starting in early afternoon local time. The peak is entirely absent on local ground stations, consistent with the general lack of detections during the day reported in the literature. However, the ocean microbarom is evident on the solar hot air balloon (elevation approximately 15 km) and prominent on the SISE/USIE balloon (elevation 34 km). The amplitude difference between the two is likely a combination of atmospheric conditions (see Eq. 4.5) and background noise. Eight of the 14 ground sensors had high-frequency wind shrouds installed, but the lack of detection on the ground is still probably due to wind noise. Alternatively, the microbarom signal could be in an elevated acoustic duct during this time and thus not reaching the ground at all.

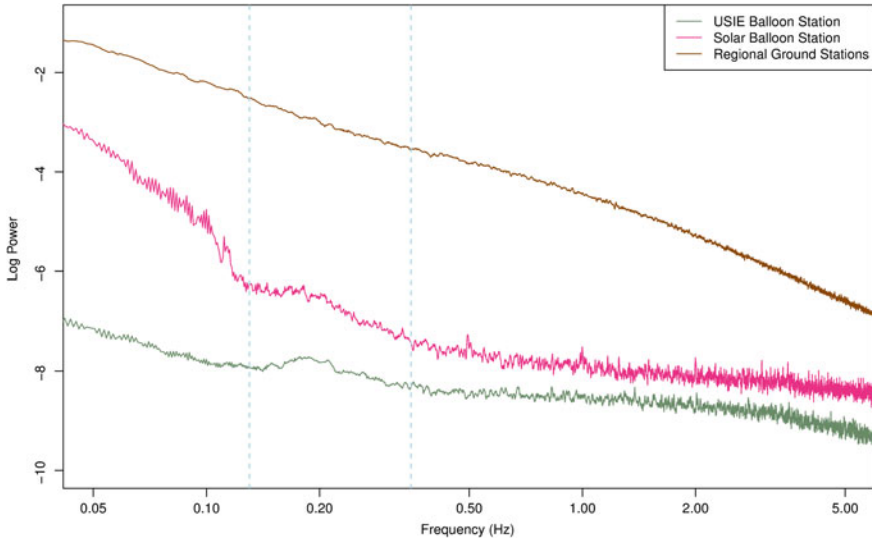


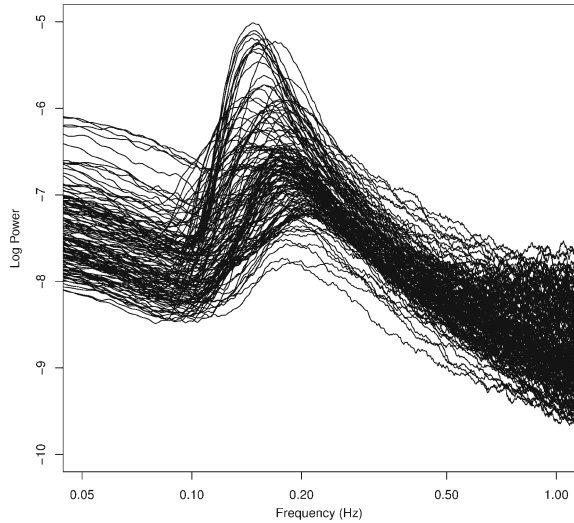
Fig. 4.12 Ocean microbarom peak recorded by airborne stations during the SISIE/USIE experiment. Each trace is a 10 min Welch spectrum from 1915 to 2345 UTC (1315 to 1745 local time), September 28, 2016. Five sensors were averaged together on the USIE balloon, one on the solar hot air balloon, and 14 channels across four locations on the ground near the balloons' flight path. Dashed blue line indicates the ocean microbarom frequency range per Campus and Christie (2010)

The microbarom is continuously recorded for the entirety of the 2016 ULDB experiment (see Fig. 4.13). The spectral power fluctuates by almost three orders of magnitude, indicating the possibility that the sensors flew very close to the source area during part of the flight. The peak is present throughout the day/night cycle, indicating that the lack of a microbarom peak during the day on ground stations is due to tropospheric rather than stratospheric phenomena. This is consistent with diurnal wind noise patterns.

4.4.4 Explosions

The SISE/USIE experiment was designed to test detection threshold of a free flying station with respect to distant sources. Three approximately 1000 kg TNT equivalent explosions were detonated while infrasound sensors were at float on a zero pressure balloon several hundred kilometers away. A prototype solar hot air balloon carrying a lightweight infrasound station was in flight near the zero pressure balloon as well. The zero pressure balloon was at an altitude of about 35 km, and the solar hot air balloon was at an altitude of about 15 km. Ground stations were deployed at distances of 5.8, 180, 260, 300, and 350 km, although the latter station was only active for the second two shots.

Fig. 4.13 Ocean microbarom peak recorded by the ULDB superpressure flight from Wanaka, New Zealand from May 18 to June 4, 2016. Each trace is a 10 min window Welch spectrum stacked over 3 h



The first blast was detected on the zero pressure balloon when it was 330 km away, however none of the ground stations farther than 6 km away captured the signal. This includes three stations lying between the blast site and the balloon. The station on the solar hot air balloon did not detect it either due to wind noise during ascent.

The signal recorded on the zero pressure balloon consisted of three arrivals. The first arrival traveled with a celerity of 290 m/s and the last at 280 m/s, both consistent with stratospherically refracted signals (Negraru et al. 2010).

The second blast was detected on the zero pressure balloon when it was 360 km away, and on the solar hot air balloon when it was approximately 300 km away from the source (Fig. 4.14). Ground stations 5.8 and 180 km away also detected the acoustic signal. Arrivals on the zero pressure balloon, the solar hot air balloon, and the ground station traveled at stratospheric celerities. The signal consisted of a single arrival on all four stations.

The third blast was detected on the zero pressure balloon when it was 395 km away from the source, but was not detected on the solar balloon. It was also observed on ground stations at 5.8 and 180 km away.

The SISE/USIE experiment was unique in that it detected signals from a known source. These signals resemble some waveforms detected on the superpressure balloon during its circuit of the southern hemisphere. Figure 4.15 compares the first shot in the SISE/USIE series with an event detected on the ULDB 2016 when it was about 1700 km east/southeast of New Zealand. The signal on the superpressure balloon is lower amplitude and lower frequency than that on SISE/USIE, but the time gap between the first and second arrivals is similar (15 s vs. 20 s). The rarefaction (negative) phase of the first arrival is higher amplitude than the compressional (positive) phase) on both balloons. The second arrival appears shorter and more impulsive than the first arrival. The presence of multiple phases and large rarefactions

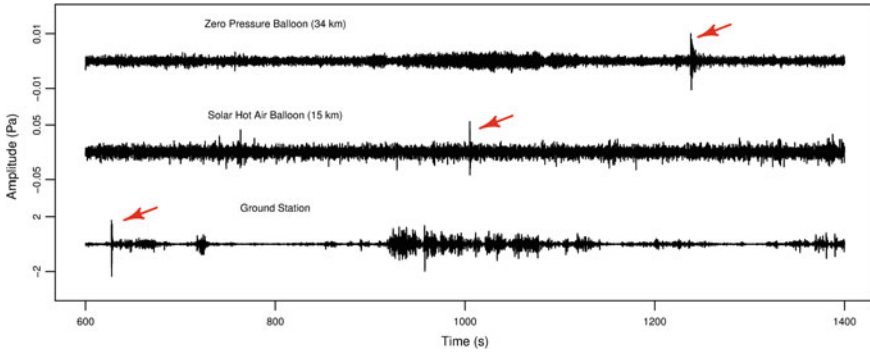


Fig. 4.14 A distant explosion captured by a solar hot air balloon in the upper troposphere and a zero pressure balloon in the middle stratosphere during the SISE/USIE experiment

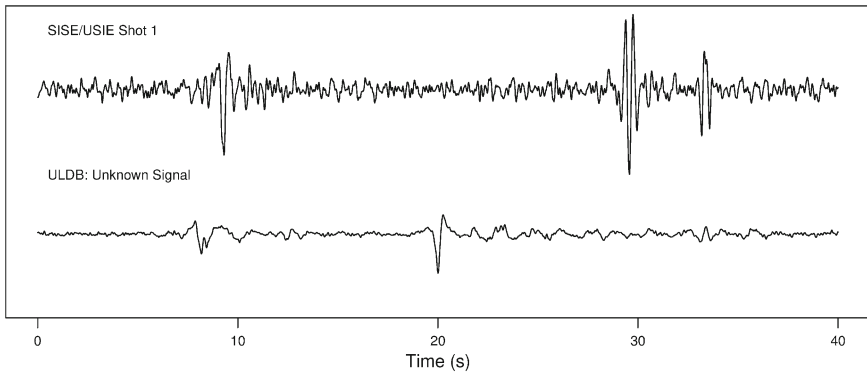


Fig. 4.15 The first shot in the SISE/USIE series recorded on a zero pressure balloon at 35 km elevation compared to a signal detected on the ULDB superpressure balloon. Peak-to-peak amplitude for the top and bottom signals were about 0.066 and 0.035 Pa, respectively

suggest that these signals are traveling along multiple paths through the atmosphere, some of which involve postcritical reflection. The lower frequency of the superpressure balloon signal indicates that the source was larger and/or further away than the SISE/USIE shot. However, the provenance of this waveform is highly speculative at present.

4.4.5 Other

The HASP 2016, SISE/USIE, and ULDB flights recorded many pressure fluctuations of unknown origin. Since data from these experiments were retrieved shortly before the time of writing, a detailed analysis of these events has not yet been performed.

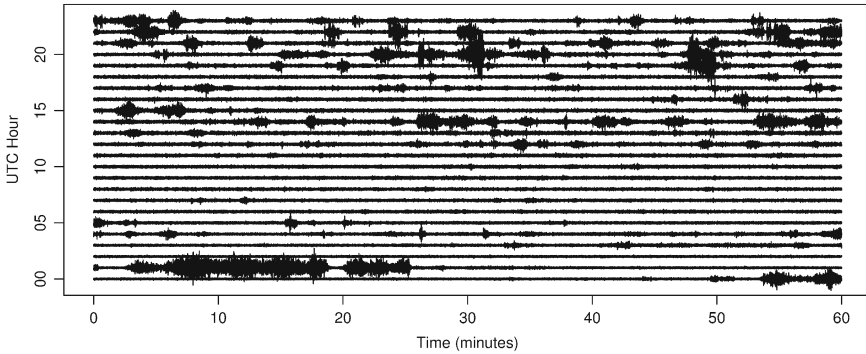


Fig. 4.16 A day of waveforms recorded on the ULDB. The trace starts at 00 UTC on May 29, 2016. Data were band passed between 0.1 and 5 Hz

In general, the events have frequencies below 10 Hz and occur anywhere from less than one to several per hour on the HASP 2016 and USIE/SISE flights.

Figure 4.16 shows pressure fluctuations recorded during 1 day of the ULDB flight. Although activity is quite variable on a tens of minutes timescale, pressure amplitudes seldom exceed 0.1 Pa peak to peak. Analysis of spectrograms indicates that there are several types of event occur during the flight. Several low-frequency (<5 Hz) broadband events occur per hour, typically lasting around 10 s or less. Discrete bursts that span the infrasound range can occur up to around 10 times per hour, though several hours can pass without a single one. There are a few episodes of sustained broadband events lasting up to 45 min as well, with most energy below 10 Hz. The occurrence of sporadic events below 5 Hz several times per hour is consistent with observations made by Wescott (1964a), but the other types were not mentioned. A definitive explanation for these pressure fluctuations awaits detailed analysis and perhaps future flights with anemometers and accelerometers on board. Cameras could also identify local disruptions to the flight system that generate pressure signals or even image a distant event responsible for an infrasound arrival.

4.5 Noise Sources, Detection Thresholds, and Other Considerations

4.5.1 Noise

Wind is the biggest contributor to noise levels on ground geoacoustic sensors in most locations (Walker and Hedlin 2010). However, a free floating balloon at neutral buoyancy in a stratified atmosphere is advected at the mean wind speed and experiences minimal differential air flow. Sources of localized wind, such as shear across the

flight line, gravity waves, balloon oscillations, and turbulence also appear to be minimal as well. Indeed, the effect of fluid motion on free flying microphones appears to be rarely, if ever, a consideration.

The current state of understanding posits three sources of noise on geoacoustic sensors during level flight: electromagnetic interference, instrument self-noise, and unwanted pressure fluctuations. Issues with electromagnetic interference and mitigation strategies are discussed in Sect. 4.3.2.2 and will not be repeated here. Instrument self-noise denotes the level of interference generated by the sensor, digitizer, and power system in the absence of external signal sources. It can be reduced by increasing the digitizer gain and/or voltage output of the sensor. A simple way to quantify this is to include one microphone that is identical to the others, except that its ability to record pressure has been curtailed. This can be accomplished by removing the mechanical filter on an InfraBSU microphone as previously described.

Self-noise was an issue on the HASP 2016, for example. Figure 4.17 indicates that the self-noise of the digitizer on the flight ladder (Trimble Ref Tek 130, gain of 32) is much higher than that on the gondola (Omnirecs Datacube at gain of 64). Signal levels on the two active gondola microphones are similar to the mechanically disabled gondola microphone above about 1 Hz, indicating that the detection threshold above this frequency is determined by digitizer noise and electromagnetic interference. Microphone pairs on the gondola and the flight ladder were mechanically reversed to isolate outside electronic interference as described in Sect. 4.3.2.2. For a microphone pair M_+ and M_- in which pressure response polarity has been flipped, non-pressure signals common to both can be eliminated to create a denoised microphone M_d

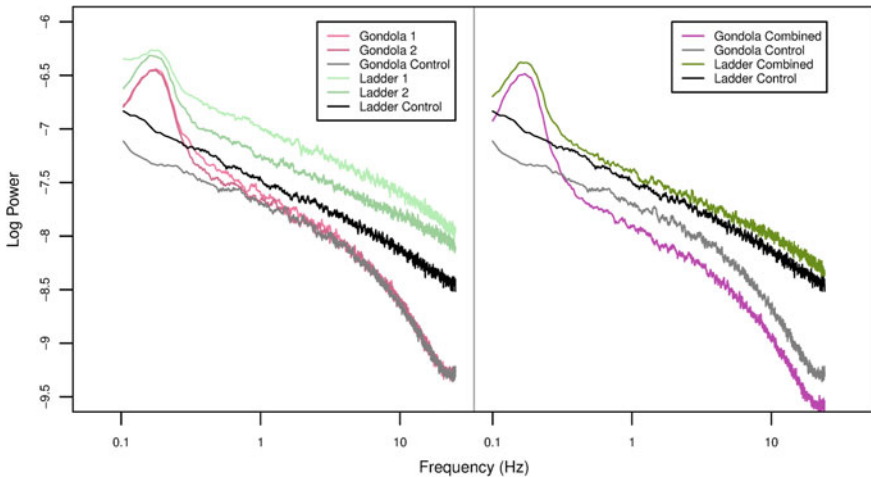


Fig. 4.17 Operational and intentionally disabled “control” microphones on the gondola and flight ladder of the HASP 2016 flight (left panel) compared to operational microphones combined into a single channel via Eq. 4.4 versus control microphones (right panel)

$$M_d = \frac{M_+ - M_-}{2}. \quad (4.4)$$

The result is to increase the sensitivity of the denoised gondola microphone above that of the control channel (Fig. 4.17). the same operation applied to the ladder microphone pair does improve the sensitivity, but not to the same extent as on the gondola microphones. This suggests a simple $\sqrt{2}$ noise reduction produced whenever two sensor channels are averaged together, indicating that the noise on the ladder is internally rather than externally generated.

Pressure fluctuations from temperature and altitude variations can produce long period signals that tend to fall in the gravity wave range. Signals near the balloon resonance frequency and in the microbarom band will be obscured as well. Beyond this, the nature of the acoustic background in the free atmosphere is poorly understood at present. Wescott (1964a) reported root mean square (RMS) acoustic amplitudes of between 0.003 and 0.1 Pa just below 1 Hz with diurnal variations. The acoustic source was believed to be turbulence in the troposphere. The noise floor from electromagnetic interference and digitizer self-noise appears to be higher than background acoustic noise during recent flights (recall Fig. 4.17).

4.5.2 Detection Thresholds

The difference in amplitude of an acoustic wave measured at two different elevations depends on the density, pressure, and speed of sound at each location. The pressure amplitude ratio θ of an acoustic wave traveling from point 1 to point 2 is proportional to the square root of the inverse ratio of their acoustic impedances:

$$\theta = \sqrt{\frac{c_2 \rho_2}{c_1 \rho_1}} \quad (4.5)$$

where ρ is density and c is the speed of sound (Rayleigh 1894; Banister and Hereford 1991). When comparing pressure amplitude of acoustic waves measured on ground stations to those measured at least one wavelength above the Earth's surface, amplitude doubling due to reflection must be taken into account as well. Thus, the pressure amplitude A_1 on the ground is related to the pressure amplitude A_2 in the atmosphere by

$$A_2 = A_1 \frac{\theta}{2}. \quad (4.6)$$

It is instructive to construct a reference pressure amplitude of an acoustic wave measured at the Earth's surface using ambient pressure, temperature, and density values at sea level set forth in the U. S. Standard Atmosphere (NOAA 1976). Then Eq. 4.6 becomes

$$A_2 = A_1 \frac{\sqrt{c_2 \rho_2}}{4l} \quad (4.7)$$

where sound speed is in meters per second, and density is in kilograms per cubic meter. Note that this includes the ground reflection adjustment described above. Accordingly, an acoustic wave measured on a ground station at sea level and again at an altitude of 35 km will suffer a 26-fold pressure amplitude reduction from this effect alone. However, this model is simplistic and probably too conservative. It does not take into account atmospheric waveguides and focusing, which can greatly enhance signal amplitudes in certain regions. The true attenuation factor is likely quite variable depending on the atmospheric profile and propagation path of the acoustic wave.

Figure 4.18 suggests that the actual signal-to-noise ratio on the HASP 2016 balloon is comparable to that of ground stations in the area when the adjustment factor θ is applied. However, the presence of the microbarom peak on the balloon but not on the ground suggests that the free flying station actually performs better in the 2-second period range. Indeed, the balloon outperforms the low-noise ground station below 1 Hz and the higher noise (less protected) station below about 8 Hz. The microphones and data acquisition system on the balloon were relatively cheap, low-end models; replacing them with lower noise floor instruments could have further improved signal quality on the HASP 2016.

Noise sources on free flying stations are composed of

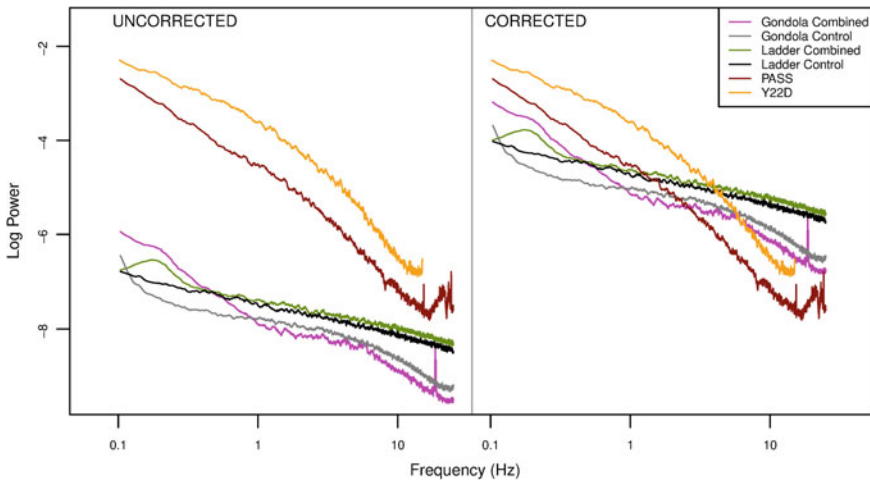


Fig. 4.18 Denoised and reference microphones on the HASP 2016 flight compared with ground stations in the area. The left panel shows the balloon microphone spectrum uncorrected for atmospheric conditions, and the right panel shows the spectrum adjusted for pressure, density, and temperature effects per Eq. 4.5. Spectra were generated using data recorded as the HASP 2016 passed almost directly over co-located ground stations PASS and Y22D. PASS had a wind mitigation system consisting of four 15 m long soaker hoses, and Y22D had no wind protection. Balloon data were scaled to the altitude of the ground stations using the 1976 Standard Atmosphere (NOAA 1976)

$$\epsilon = \epsilon_w + \epsilon_p + \epsilon_e + \epsilon_s + \epsilon_v + \epsilon_a \quad (4.8)$$

where ϵ_w is from wind noise, ϵ_p is from non-hydrodynamic pressure fluctuations (barometric, temperature, and elevation changes), ϵ_e is outside electromagnetic interference, ϵ_s is internal sensor/digitizer noise, ϵ_v is sensor motion (i.e., vibration) and ϵ_a is undesired acoustic waves. On the ground,

$$\epsilon_w \gg \epsilon_p + \epsilon_e + \epsilon_s + \epsilon_v + \epsilon_a \quad (4.9)$$

at frequencies above several tens of seconds. On balloons, $\epsilon_w \approx 0$. The contribution ϵ_p is typically a very long period on ground and free flying stations, although balloons suffer high levels just below the Brunt–Vaisälä frequency due to resonance. Noise on balloon-borne stations appears to consist of contributions from ϵ_e and ϵ_s as noted above, particularly at higher frequencies. Bowman and Lees (2015a) did not find evidence of vibration noise ϵ_v during the first HASP flight, and later results are consistent with this conclusion. This is probably due to the stability of balloon systems at float combined with very low motion sensitivity of the InfraBSU microphones included in each experiment (Marcillo et al. 2012). The ocean microbarom is a near constant source of ϵ_a in the 5 s period vicinity during balloon flights and sometimes on the ground as well.

The signal-to-noise ratio (SNR) of a single geoacoustic sensor with respect to unity amplitude can be expressed as

$$\text{SNR} = \left(\frac{1}{\epsilon_n + \epsilon_a} \right)^2 \quad (4.10)$$

where

$$\epsilon_n = \sum \epsilon_w + \epsilon_p + \epsilon_e + \epsilon_s + \epsilon_v \quad (4.11)$$

is the total contribution of non-acoustic noise. Since acoustic noise ϵ_a and signals of interest suffer the same attenuation factor θ with changes in atmospheric conditions, Eq. 4.10 can be rewritten as follows:

$$\text{SNR} = \left(\frac{1}{\theta \epsilon_n + \epsilon_a} \right)^2. \quad (4.12)$$

Thus, θ is more properly thought of as an enhancement of non-acoustic noise rather than an attenuator of acoustic signals as far as detection thresholds are concerned.

For an ideal geoacoustic sensor, $\epsilon_n \rightarrow 0$, and thus the value of θ is nugatory. Such an ideal sensor cannot exist at the Earth's surface due to the unavoidable influence of ϵ_w . The task of reducing ϵ_e and ϵ_s is much more tractable, however, which suggests that a free flying station could approach the theoretical upper limit of acoustic sensitivity described above. The region in which ϵ_a is lowest is likely the stratosphere because it is far from localized acoustic sources at the Earth's surface and is generally less turbulent than the troposphere.

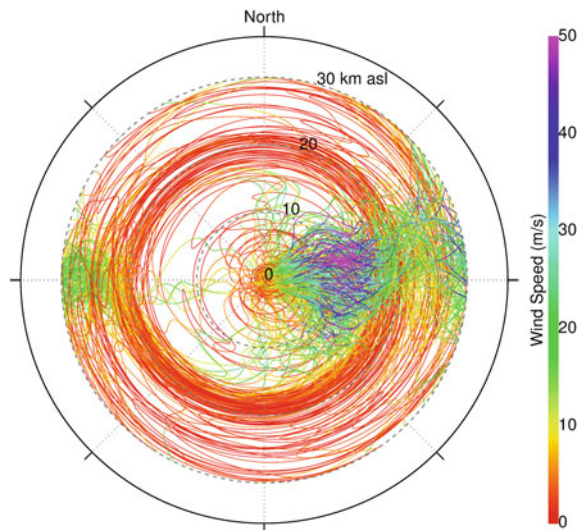
4.5.3 Other Considerations

4.5.3.1 Station Keeping

The atmosphere is in constant motion, and anything embedded in it will not remain in the same location for long. This can be an advantage, since free flying stations can sample large regions in a matter of days. For example, the 2016 ULDB flight circumnavigated the Earth in 2 weeks. However, attempts to target specific phenomena can be difficult because the trajectory of the geoacoustic station depends on wind velocities at all elevations between launch and float altitudes. For example, the SISE/USIE balloon was supposed to fly westward from the launch facility and pass within 100 km of the blast site. Since the launch was delayed for several weeks, the biannual reversal of stratospheric winds actually carried the balloon east, resulting in a much greater range (over 300 km).

Flight paths can be planned with reasonable accuracy by utilizing variations in wind fields at various altitudes. Figure 4.19 shows wind profiles in the mid-latitudes over 1 year. Strong winds between 5 and 15 km above sea level permit rapid eastward motion most of the time. Winds between 15 and 22 km tend to be light and variable, allowing a station at this altitude to drift only a few kilometers per hour. Above about 22 km, the stratospheric winds carry stations east during the summer and west during the winter. A flight system with the ability to change altitude can remain relatively stationary by utilizing the opposing summer stratospheric and tropospheric winds to shift back and forth.

Fig. 4.19 Wind profiles above Chapel Hill, North Carolina, USA generated from Global Forecast System analysis model runs (Bowman and Lees 2015b)



4.5.3.2 Doppler Shift

Since free flying stations are almost always moving with respect to stationary acoustic sources, the resulting signal experiences a Doppler shift. The frequency f_r of the Doppler-shifted signal is related to the original frequency f , the speed c_b of the balloon, the local sound speed c_s at the balloon, the signal-receiver back azimuth θ_b , the balloon motion azimuth θ_m and the source- balloon elevation angle ϕ via

$$f_r = \frac{f}{1 + (c_b/c_s) \cos(\theta_b - \theta_m) \cos \phi} \quad (4.13)$$

This expression was adapted from Lighthill (1978). Thus, a 10 Hz ground source recorded by a balloon moving at 20 m/s could be shifted up to 10.7 Hz (approaching) or down to 9.4 Hz (receding) assuming a sound speed of 304 m/s in the stratosphere.

While the Doppler shift can obscure the true frequency content of signals recorded on balloons, it also can be useful in certain situations. For example, a Doppler-shifted transient signal recorded on two balloons some distance apart will provide the necessary constraint to define a unique source location, provided the sensors are moving in different directions. Also, a single free flying station can localize the source of a persistent signal if it lasts a sufficient amount of time.

4.5.3.3 Direction of Arrival

Acoustic arrays are a powerful tool in ground-based geoacoustic monitoring, but deploying them in the free atmosphere is difficult. Vertically oriented linear arrays are the simplest to construct and were used to good effect by Wescott (1964a). Smaller vertical arrays were deployed on the HASP flights as well. This sensor distribution can measure the angle of incidence of up and down going waves, but they cannot distinguish azimuth. A horizontal array with the necessary aperture for azimuth discrimination would need to be several tens of meters across. Such a contraption could not be launched, but perhaps could be unfolded once float is attained. In any case, the engineering challenges are formidable.

Another possibility is to utilize multiple flight platforms. The SISE/USIE experiment demonstrated this by recording a far-field explosion on two stations at different locations and altitudes (recall Fig. 4.14). In another case, two identical superpressure balloons launched minutes apart stayed within 200 km of each other for 14 days (Lally 1967). Thus, it is possible to have the floating equivalent of a regional geoacoustic array for several weeks at a time, although the network will eventually drift apart. Since the sensor spacing would almost certainly be greater than the acoustic wavelength, array processing methods such as the grouping technique of de Groot-Hedlin and Hedlin (2015) would be required.

Finally, a sensor that could detect air motion associated with a passing acoustic wave would permit direction of arrival determination. This is conceptually equivalent to a P-wave arrival on a seismometer. Proposed designs have included measuring

the motion of the flight system as a result of an impinging wave, acoustic gradiometry, and precise sampling of the wind field. However, none of these have advanced beyond the conceptual stage.

4.6 Applications

4.6.1 *Treaty Verification and Natural Hazards Monitoring*

The International Monitoring System (IMS) was developed to enforce the Comprehensive Nuclear-Test-Ban Treaty (CTBTO). The IMS consists of a global network of seismic, hydroacoustic, radiological, and infrasound stations tasked with detecting and characterizing clandestine nuclear blasts. When the network is complete, the infrasound component will comprise 60 stations. As of this writing, 49 are certified, 3 are under construction, and 8 are in the planning stages. Simulations indicate that explosions with yields greater than 420 tons nuclear equivalent will be detected over 95% of the Earth with a probability of 90% or greater (Green and Bowers 2010) once the IMS is complete. This fulfills the design goals of the network (Christie and Campus 2010).

In addition, infrasound has recently become a useful means of determining if a volcanic eruption has occurred (Matoza et al. 2017). This is because infrasound is produced only when an eruption is in progress, unlike seismic activity that is not necessarily associated with material ejection (Fee and Matoza 2013). Recently, Tailpied et al. (2016) demonstrated the efficacy of the IMS for monitoring Yasur volcano in the south Pacific and Etna volcano in the Mediterranean, and Fee et al. (2016) utilized infrasound recorded on seismometers to characterize eruptions on remote volcanoes in the Aleutians. Tsunamis also generate powerful infrasound signals (Le Pichon et al. 2005), which could provide amplitude estimates and early warning if captured before they make landfall.

Despite the robust nature of the IMS network, there are logistical and environmental issues that can affect its detection capability. For example, there are regions of the southern ocean that are 3500 km from the nearest land, creating a 7000 km gap in ground network aperture. Stations on remote islands suffer from high levels of wind noise, further degrading detection capabilities in large maritime regions. Sensors located in desert areas often suffer severe wind noise during the day, whereas those at high latitudes may experience high wind noise at any time (Christie and Campus 2010). Variability in stratospheric winds can have a large impact on detection capability, particularly in the tropics (Le Pichon et al. 2012). Local sources of coherent infrasound increase clutter on some stations also (Matoza et al. 2013).

Balloon-borne stations are unaffected by wind noise, removing one of the major impediments to far-field acoustic signal detection. They are able to travel over the open ocean, providing coverage where land stations cannot (recall Fig. 4.3). Balloons can be placed in elevated acoustic ducts, where they can detect signals that

never reach the ground. Finally, they are far from local infrasound sources at the Earth's surface. They would be particularly effective in the tropics and over the southern oceans, where atmospheric conditions and lack of ground station coverage can degrade IMS detection capability (see Fig. 5 in Le Pichon et al. 2012 and Fig. 5 in Green and Bowers 2010). Stations drifting near remote volcanoes can provide eruption detection capability, which is critical for those that lie near aircraft flight paths. Balloons over ocean basins might provide a detection system for tsunamigenic infrasound also.

Small superpressure balloons can remain in the stratosphere for over 2 years (Lally 1991). Geoacoustic sensor platforms on such balloons could be launched from southern regions such as New Zealand, where they would circle the Earth every couple of weeks. A succession of launches could ensure sensor spacing of several thousand kilometers, improving the 7000 km gap described above. Balloon motion also would provide a constraint on acoustic velocity in these poorly instrumented regions. A similar network could be deployed near the equator. Furthermore, stations could be deployed in response to specific operational or atmospheric conditions (e.g., loss of an IMS station, decreased detection capability during the biannual stratospheric wind reversal).

The development of a permanent balloon-borne geoacoustic network would require investments in launch facilities, data telemetry, and new analysis techniques. Their tendency to drift off course would result in inevitable network degradation over time. Indeed, the constantly changing position implies that the network configuration would only be known a week or two in advance. Despite these challenges, the motivation and technology required to realize a free flying network already exist.

4.6.2 *Bolide Detection*

Stratospheric infrasound sensors can monitor the flux of space-borne objects that burn up in the Earth's atmosphere. The Chelyabinsk bolide was a prime example: 20 IMS infrasound stations sensed the 460 kt TNT equivalent explosion, and some of them even recorded the waves on their second circuit around the globe (Le Pichon et al. 2013). Smaller bolides are regularly detected by satellites that monitor the flashes resulting from their burn-up in the atmosphere since about 10 % of the energy of a bolide's explosion is emitted as optical or infrared light (Brown et al. 2002a). The Jet Propulsion Laboratory's Fireball and Bolide web page (Jet Propulsion Laboratory 2016) currently reports a few events per month with energies down to 0.1 kt TNT equivalent (see Fig. 4.20).

Balloon-borne geoacoustic stations may improve sensitivity to bolides at the small end of the Near-Earth Object (NEO) distribution of impactors. While the amplitude of a pressure wave does decrease as the ambient pressure itself decreases (recall Eq. 4.5), the lack of wind noise greatly improves the signal-to-noise ratio. Furthermore, bolide explosions typically take place between 20 and 30 km altitude (Edwards et al. 2006), where the energy of the explosions may be efficiently trapped

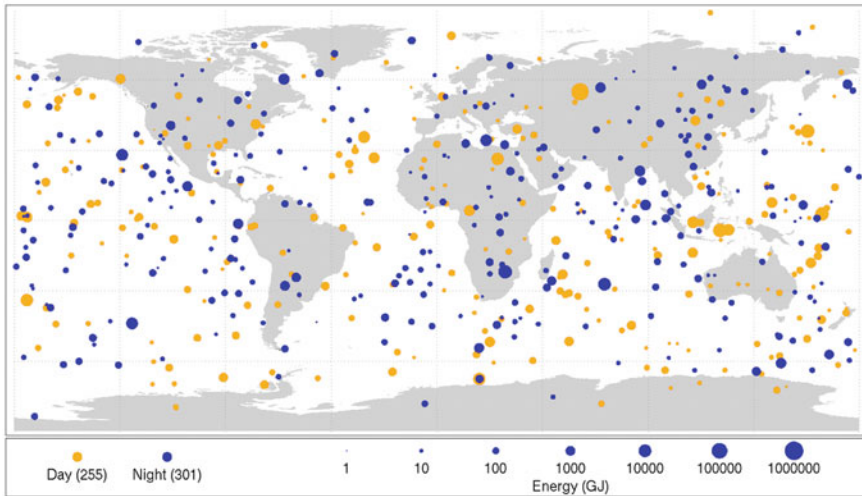


Fig. 4.20 A map of 556 bolide detections between 1994 and 2013 with associated optical energies. Note that the population below 1 kt TNT equivalent is likely very underrepresented. About 30% of the 0.1 kt TNT equivalent bolides were seen on the IMS infrasound network as well. Image credit: NASA

in a stratospheric duct. Finally, the strength and density of the bolide may translate into acoustic signatures that can distinguish between distinct NEO impactor populations.

Period-yield relations originally developed for infrasound signals from nuclear blasts also provide a robust measure of the total energy of bolide events (Brown et al. 2002b). A NEO traveling at 3 km/s has kinetic energy approximately equal to twice its mass in TNT. The minimum impact velocity is 11 km/s (the Earth's escape velocity), and some NEOs have velocities that are significantly higher. As an example, a 0.1 kt event (total impact energy) results from a 4500 kg object traveling at 14 km/s. If this object had a density of 2.7 g/cm^3 (like granite), then its size would be equivalent to a 165 cm cube. In fact, balloon-borne infrasound sensors could detect much smaller energies. For example, the SISE/USIE experiment (see Sect. 4.2.1.4) successfully detected two explosions with the kinetic energy equivalent of a 50-kg NEO impacting the Earth's atmosphere at 14 km/s.

The prospects for bolide infrasound detection using a network of long-duration balloon-borne platforms bear further study. There are some basic questions at present: what is the optimum range in altitude for best sensitivity to bolides? How are bolide-generated infrasound waves likely to propagate in the stratosphere? What distribution of balloons is necessary to provide sufficient sensitivities around the globe? Nevertheless, it seems that a network of infrasound sensors on small, long-duration superpressure balloons may improve our sensitivities to small NEO impactors by an order of magnitude or more.

4.6.3 Upper Atmosphere Energetics and Ionospheric Disturbances

Up going acoustic waves carry energy into the upper atmosphere, where they dissipate as heat. Calculations by Rind (1977) indicate that the ocean microbarom can heat the 100–140 km region by over 30 K per day. Analysis by Hickey et al. (2001) also predicts thermospheric heating on the order of tens of Kelvin, although acoustic waves do not appear to heat the mesopause region (Pilger and Bittner 2009). The elevation at which acoustic heating occurs is dramatically lower for narrow band acoustic waves due to nonlinear effects (Krasnov et al. 2007).

Acoustic and acoustic-gravity waves of sufficient amplitude can perturb the ionosphere, producing fluctuations that can be detected using ground-based GPS (Cahyadi and Heki 2015) and continuous Doppler sounders (Krasnov et al. 2015). These disturbances have been generated by rockets (Mabie et al. 2016), earthquakes (Krasnov et al. 2015), tsunamis (Wu et al. 2016), explosions (Drobzheva and Krasnov 2003), and thunderstorms (Davies and Jones 1973), among others. While the detection and characterization of ionospheric disturbances have obvious implications for the remote monitoring of natural hazards, open questions remain about the relationship between the acoustic source and resulting high-altitude fluctuation. For example, Chum et al. (2012) found that predicted values for air motion in the ionosphere were two times higher than those measured from infrasound during the Tohoku earthquake.

Free flying sensors in the troposphere and stratosphere are able to intercept up going acoustic waves as they travel from their source to the upper atmosphere, providing a critical constraint that cannot be measured on the Earth's surface. Indeed, measurements of the acoustic background noise as well as a possible direct overflight of the ocean microbarom during the 2016 ULDB experiment may provide the first glimpse of the energy flux from the stratosphere into the mesosphere and beyond. However, it is likely that the acoustic background varies by location and time of year. Also, the ULDB sensor package cannot determine the direction of arrival of the signals. Experiments designed to measure up going acoustic flux should include a vertically oriented linear array and take place in several locations over different seasons.

4.6.4 Signals Inaccessible to Ground Sensors

In general, the acoustic velocity profile of the troposphere causes infrasound signals to refract away from the Earth's surface. The prevalence of wind noise also limits infrasound detection thresholds, particularly during the day (Bowman et al. 2005). This suggests that balloon-borne platforms might be a better venue for long-term studies of phenomena such as the ocean microbarom. For example, Rind (1977) investigated the thermospheric tide's effect on ocean microbarom propagation but

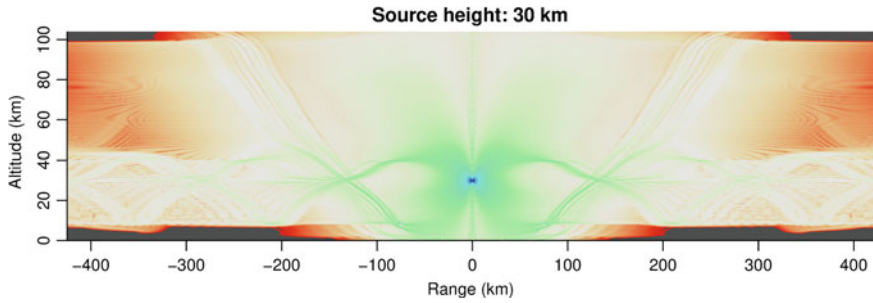


Fig. 4.21 Simulation of transmission loss from a 1 Hz acoustic source at an elevation of 30 km using atmospheric data from September 28, 2016 over central New Mexico. The cross section is oriented East–West

noted that surface winds prevented observations 10 to 30% of the time. In contrast, the ocean microbarom is nearly constant on high-altitude balloon deployments.

Infrasound signals generated by wind flow over mountains (Walterscheid and Hickey 2005) or during thunderstorms (Farges and Blanc 2010) may be difficult to observe due to adverse ground conditions. Furthermore, they may be directional in nature; the “charge contraction” signal during lightning discharge is one example (Balachandran 1983). Sensors in the stratosphere may provide unique insights into the acoustic wave field from these phenomena.

Propagation models suggest that acoustic sources near the tropopause may generate signals that travel in an elevated, bidirectional duct (see Fig. 4.21). Waves trapped in this duct may propagate to much greater distances than those elsewhere, making this a possible analog for the SOFAR channel in the ocean. Phenomena that could generate infrasound in this region include thunderstorms, bolides, and rockets. The presence of thunderstorms during flights in 2014 and 2015 but not 2016 offers a tentative acoustic explanation for the unusual signals described in Bowman and Lees 2015a (recall Fig. 4.8), although it is difficult to understand how they could have been generated.

4.6.5 *The Exploration of Venus*

Recently, researchers have begun to explore the possibility of conducting infrasound measurements from balloons floating in the atmosphere of Venus. This section is concerned with what motivates this interest, the acoustic properties of Venus, and progress in addressing the key technical questions that must be solved before a Venus balloon infrasound mission is conducted.

4.6.5.1 Why Explore Venus with Balloon Infrasound?

During the 50 years of planetary exploration, researchers have exploited the electromagnetic spectrum very thoroughly making observations from gamma rays to very low frequency radio waves. However, there has been no attempts to use infrasound for planetary exploration.

The primary driver for considering infrasound is the dense atmosphere of Venus that precludes orbital remote sensing observations of the surface with electromagnetic radiation except for very limited spectral bands. This thick atmosphere also ensures that the surface is extremely hot (approaching 465 °C over broad areas) such that our twin planet also presents a formidable challenge for in situ investigations with landers and rovers.

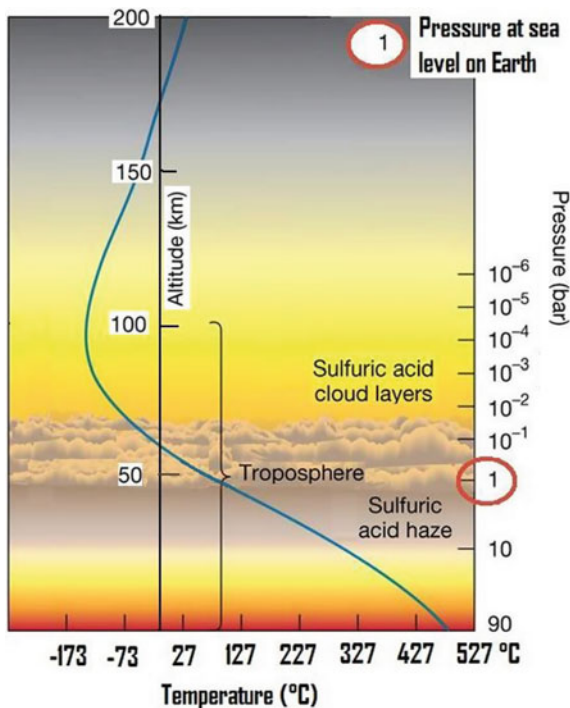
Seismology is a powerful technique that is responsible for much of what we know about the Earth's interior, has played a key role in characterizing the lunar interior, is about to be applied at Mars with the InSight mission and can play a key role in answering fundamental questions about Venus. However, seismic instruments used at the Moon and Mars will not work under Venus surface conditions (465 °C and 90 bars).

A study sponsored by the Keck Institute for Space Studies (KISS) entitled “Venus Seismology” conducted in 2014 and published in March 2015 (Stevenson et al. 2015) explored alternative techniques that can be implemented from balloons floating high in the Venus atmosphere, where temperatures are comparatively benign or from Venus orbit. A workshop was held in June 2014 in which three coauthors participated unaware that at virtually the same time other coauthors were initiating an effort to revive geoacoustic investigations using balloons on Earth. The report on the KISS study published in March 2015 concluded that infrasound generated by quakes on Venus can be observed either directly from balloons floating high in the atmosphere or indirectly by monitoring infrared radiation from a spacecraft orbiting Venus. Moreover, because of the dense atmosphere of Venus, the signals from an event of a given size were almost two orders of magnitude larger than they would have been for a terrestrial balloon. Explosive volcanic events on Venus could also be observed with infrasound signals although this possibility was not explored in any detail. The next section focuses on the balloon infrasound observations and includes a discussion of how to determine if Venus is seismically active and if so to explore the interior structure of Venus using infrasound measurements.

4.6.5.2 Venus Atmosphere Characteristics and Balloon Flight

The atmospheric temperature and density profiles of Fig. 4.22 indicate that the average surface temperature is about 465 °C and the pressure is 90 bars—the equivalent of a depth of about 1 km of seawater. With increasing elevation, the temperature and pressure both decrease steadily and an altitude of 55 km, the pressure is about 500 mb and the temperature is about 40 °C. In 1985, two Soviet VEGA balloons were deployed in the Venus atmosphere and floated near 55 km. Each was tracked from

Fig. 4.22 Density and temperature profile of the Venusian atmosphere



Earth for 2 days before their batteries were exhausted (Blamont 1985; Sagdeev et al. 1986).

Venus also differs profoundly from Earth in other ways. Unlike the Earth and Mars which spin on their axes with very similar periods (Mars is 24 h and 40 min) and with their spin axes tilted to their orbital planes, Venus rotates very slowly in a direction that is opposite to its orbital motion and the Venus day (243 earth days) is longer than its year (225 days). Moreover, the spin axis is essentially orthogonal to its orbit and so there are no seasons. These differences have consequences for the atmospheric circulation on Venus.

In contrast with the very slow rotation of the surface of Venus, the atmosphere at balloon altitudes is in very rapid motion (super-rotation) with a zonal flow of approaching 100 m/s relative to the surface. Based on the VEGA balloon tracking there is also a modest motion in a meridional direction that is most likely due to a result of Hadley cell circulation. Based on what currently is known about Venus, a balloon deployed near the equator would circumnavigate the planet every 5 days and gradually drift irregularly toward the nearest pole in a time period of a month or perhaps more. As a result, infrasound observations would be conducted over the better part of hemisphere in the course of a 1-month mission, which would be terminated by loss of solar power at high latitudes.

Fig. 4.23 Venus balloon prototype (5.5 m diameter, 4.5 kg payload capacity). The balloon includes an exterior Teflon film for protection from sulfuric acid in the Venus clouds



During the past two decades, the Jet Propulsion Laboratory (JPL) has been investigating a number of different approaches to the design of Venus balloons. At this time, the most mature of these is a superpressure balloon similar in concept to the Soviet VEGA balloon and the terrestrial superpressure balloons discussed in Sect. 4.3.1. A prototype of a 5.5 m balloon designed to carry a 4.5 kg payload at Venus appears in Fig. 4.23.

Tests have demonstrated that this balloon can tolerate extended exposure to the sulfuric acid mist on Venus and multiple day–night temperature cycles as the balloon repeatedly circumnavigates the planet. Several proposals have been made to NASA’s Discovery program for atmospheric investigations with this balloon without success so far. However, a flagship mission called Venus Climate Mission incorporating a superpressure balloon was included in the recommendations of the National Research Council’s Planetary Science Decadal Survey (Squyres 2011).

Other balloon concepts have also been considered for Venus, which would permit controlled excursions in altitude. Reversible fluid balloons take advantage of unique properties of the Venus atmosphere including its high temperature and molecular weight (Jones 1995). This permits the use of water and ammonia as both a buoyancy fluid and a means of controlling altitude. These fluids are more easily stored than

helium or hydrogen while in transit to Venus. More recently, the Adaptable Multi-Segment Altitude Control (AM-SAC) balloon has been devised with the capability for large-altitude excursions and periods of stable flight over widely different altitudes (de Jong 2015). As promising as these new ideas are, the baseline mission for exploring the potential of infrasound remains a helium-filled superpressure balloon deployed on entry into the Venus atmosphere.

4.6.5.3 Acoustic Sources on Venus

Potential natural sources of infrasound on Venus include seismic events, explosive volcanism, meteors, and atmospheric disturbances. Evidence for occurrences and likely magnitudes of these sources at Venus can be culled from the observations that have been collected by past missions such as Magellan and Venus Express and the currently operating Akatsuki mission. On Venus, there are no anthropogenic acoustic signatures except on the rare occasion a spacecraft enters the atmosphere. It is important to understand these levels and the characteristic signatures of the natural sources so that they can be confidently discriminated from one another.

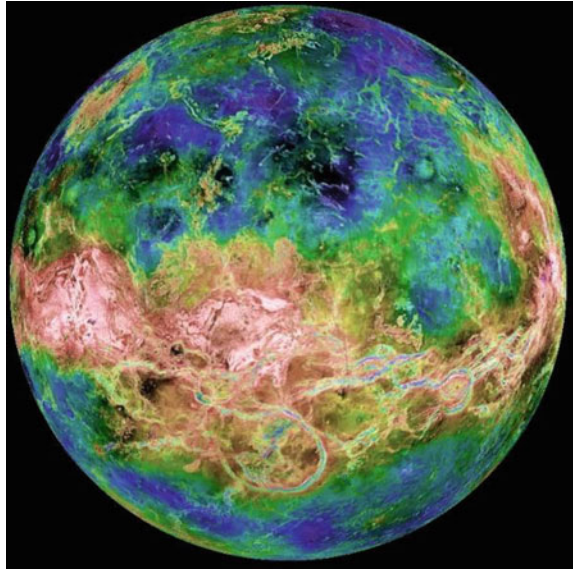
The Magellan mission mapped Venus with a synthetic aperture radar to a resolution of about 75 m/pixel. As shown in Fig. 4.24, these maps reveal a rich variety of tectonic features and widespread evidence of volcanism. The timescale for this activity remains controversial but the Venus surface appears to be much younger than Mars and the Moon. Some scientists hold the opinion that Venus was dramatically resurfaced in a single event. Others contend that these events have occurred continually through its history up to the present day (Frankel 1996).

The morphology of the structural features seen in radar images as well as the youthfulness of the planet surface testify to the potential for seismic activity. There seems to be plenty of evidence that the crust of Venus has experienced stress. However, the contemporary rate of stress release is unknown and it is possible that, as on Earth, much of it is aseismic.

Two competing conditions on Venus will influence the likelihood of stress release. On the one hand, the lack of water would result in a larger fraction of seismic energy release; on the other hand, the higher temperatures would limit the magnitude of stress release events. Quakes resulting from mineral phase changes may be also be important on Venus although they have no physical expression at the surface. The KISS study team considered that Venus was likely to be significantly less active than Earth but more active than Mars. For planning purposes, a conservative level of 25x less active than Earth was assumed. Because of the unique characteristics of the Venus atmosphere, even this low level may be readily detectable with infrasound techniques.

Venus has over 1600 major volcanoes or volcanic features, and there are many more volcanoes smaller in size. No one has yet counted them all, but the total number may be over 100,000, meaning that Venus may have more volcanic landforms than any other planet in the Solar System (Volcano World 2017). A key question is how

Fig. 4.24 Radar map of Venus based on images from NASA's Magellan spacecraft. Venus exhibits a variety of volcanic and tectonic features



many of these volcanoes are active and how active. There are currently two lines of evidence indicating continuing activity.

The first line of evidence is the occurrence of large episodic changes in the concentration of sulfur dioxide in the atmosphere. On at least two occasions since the advent of space observations, the global concentration of sulfur dioxide above the clouds has risen abruptly and has been followed by a slow decline of a factor of 10 in concentration extending over about 10 years (Marcq et al. 2013). This is believed to be consistent with a large volcanic eruption punching through the cloud layer into the Venus stratosphere followed by the gradual return to a stable condition with low SO_2 at these altitudes. However, it is not possible to rule out atmospheric instabilities as a cause.

Another line of evidence relates to the characteristics and behavior of some volcanoes as viewed in narrow infrared windows in the atmosphere (Smrekar et al. 2010). Some of these volcanoes exhibit an enhanced emissivity suggesting that they result from relatively recent flows. However, there is no way to say how recent. Other scientists have even reported actual temporal changes in the character of the flows during the Venus Express mission (Shalygin et al. 2015). Admittedly, these results are not widely accepted. With no definitive results yet on the occurrence of volcanism using conventional methods and questions about whether improvements in conventional infrared instrumentation can ever answer them (the dense atmosphere sets the fundamental limit to detecting these effects) interest is now turning to where infrasound techniques from balloon altitudes or orbit could provide an answer.

Meteors can be expected to be a source of acoustic energy just as they are on the Earth. A number of meteoroid streams impacting Earth also intersect the orbit of

Venus (Beech 1998), but there are no predictions of the rate of impacts at Venus. Actual observations of the rate using infrasound techniques would be of significant scientific interest. Meteors are believed to be important in the nucleation of the Venus clouds and so any information on the rate of meteor infall and the composition of the infalling material would be significant.

Observations from both the Venus Express and Akatsuki spacecraft have indicated the formation of gravity waves on Venus, which appear to result from atmospheric flow over topographic features (Fukuhara et al. 2017; Ando et al. 2015). These propagate into the cloud layer and would be observable at balloon altitudes. There is also indirect evidence for lightning on Venus (e.g., Russell et al. 2007) but confirmatory optical signatures are yet to be verified. If lightning does occur, it would be a potential source of infrasound (Farges and Blanc 2010).

4.6.5.4 Propagation of Seismo-Acoustic Waves on Venus

The primary motivation for infrasound investigations of Venus has been the possibility of seismic acoustic observations with the goal of understanding the level and distribution of seismicity on Venus and the possibility of probing the interior structure by exploiting the signatures from large quakes. Accordingly, more analysis has gone into understanding propagation from seismic sources than volcanoes, meteors or atmospheric disturbances.

Acoustic waves from a seismic event on Venus are coupled much more efficiently into the atmosphere than on Earth. The coupling efficiency is intermediate between that for the Earth's atmosphere and the Earth's ocean. Signals propagating from directly above the epicenter or from surface waves propagating out from the quake epicenter both travel vertically upward into the atmosphere.

Because the atmosphere is primarily carbon dioxide, attenuation is higher than it would be in an atmosphere with nonpolar molecules. As illustrated in Fig. 4.25, the attenuation is frequency dependent and only affects frequencies well above 10 Hz at the altitude of a floating platform (54 km). For observations of infrasound from an orbiting platform it may be important at much lower frequencies.

Acoustic signals originating from a Venusquake and reaching a balloon can be characterized as one of two types. The epicentral wave originating from directly above the epicenter propagates directly through the atmosphere to the site of observation. The Rayleigh wave propagates as a surface wave in the solid body of the planet. Vertical surface displacements caused by the Rayleigh wave directly beneath the balloon then propagate up to balloon altitudes. In Fig. 4.26, the analysis by Garcia et al. (2016) indicates that the surface displacements of the Rayleigh waveform are faithfully recorded in pressure variations at balloon altitudes.

Accordingly, there are several possible avenues to using balloon-borne infrasound measurements to investigate the seismicity and interior structure of Venus. Measurements of epicentral waves could make it possible to detect very small quakes on Venus ($M_e=3$) and produce a first map of global seismicity. Detection of large quakes could enable propagation times of Rayleigh waves to be measured and hence

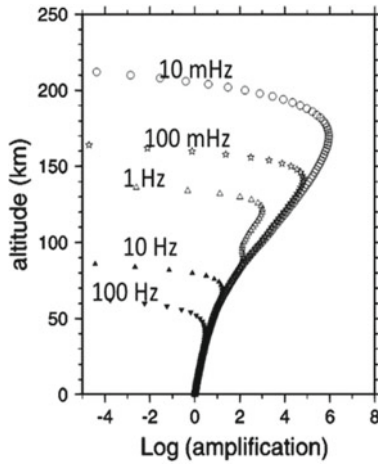


Fig. 4.25 Acoustic wave amplification as a function of altitude on Venus from Garcia et al. (2016). Frequency-dependent attenuation is insignificant at balloon altitudes

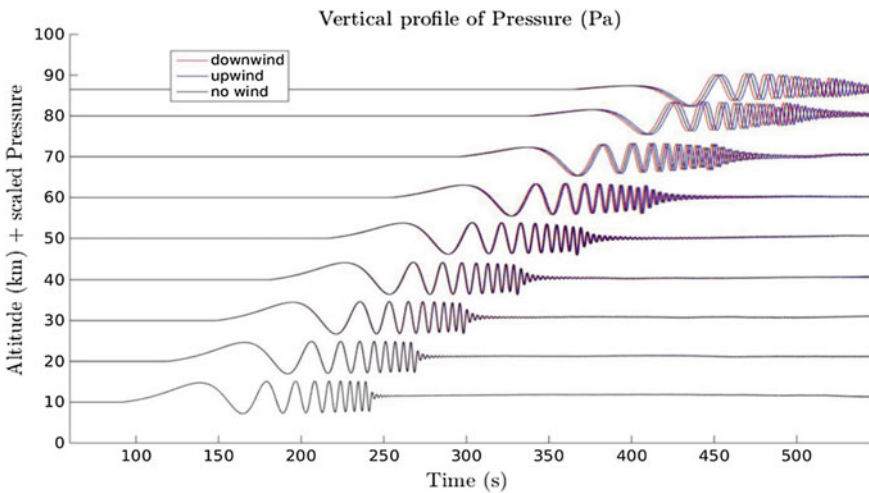


Fig. 4.26 Infrasound waveforms as a function of altitude form a faithful replica of the Rayleigh wave that drives them up to balloon altitudes (Garcia et al. 2016)

information about the planet’s interior to be gathered. The preferred approach for this would be a network of balloons that could observe the seismo-acoustic signatures of the same event at several locations around the planet. However, there is a more remote possibility of using the single seismic station approach that is being pioneered by the Mars Insight mission (Lognonné et al. 2012).

4.6.5.5 Venus Quake Detection

Infrasound pressure signals emanating either directly above the epicenter of a seismic event or from the Rayleigh waves would be detected by sensors located on a balloon floating in the favorable environment of the middle atmosphere of Venus near 55 km altitude. Discrimination of epicentral signals originating from quakes from other sources and background will be a challenge. The baseline approach is to deploy two or more microbarometers on a tether beneath the balloon. Comparisons of the signals between the sensors would be used to discriminate pressure variations resulting from an upwardly propagating wave from the surface from the effects of altitude changes due to updrafts and downdrafts and changes in buoyancy of the balloon. On the other hand, an acoustic arrival with frequency dispersion will represent strong evidence of Rayleigh wave excitation. That is because dispersive acoustic waves are relatively rare and tend to form within low elevation waveguides (Herrin et al. 2006; Negraru and Herrin 2009); such a wave train would be invisible to a high altitude balloon. Lamb waves also exhibit dispersion, but are confined to low altitudes as well (Bretherton 1969). Other sensing approaches being explored include the use of sensitive accelerometers on the pole pieces of the balloon to measure the response of the balloon to the passage of an acoustic wave, which may make it possible to detect the azimuthal direction of the wave. The platform would circumnavigate Venus every five days enabling a survey of Venus seismicity.

Infrasound originating from quakes may also be detected as a modulation of air-glow signals at 1.27 and 4.3 μm . These signatures could be detected from a Venus orbiter, but likely not from ground or space based platforms near Earth. Complementary observations of the same event at the much higher frequencies that are possible from in situ platforms on the surface and in the middle atmosphere would greatly enhance the ability to survey seismicity and probe the Venus interior.

4.6.5.6 Earth as a Testbed for a Venus Balloon Infrasound Experiment

Venus is not the place to begin experimenting with different techniques for measuring infrasound. Accordingly, JPL in collaboration with the Institut Supérieur de l'Aéronautique et de l'Espace (ISAE) of Toulouse, France has begun a program of test flights intended to validate techniques for detecting Venus quakes using Earth as an analog environment. The initial tests will involve sensors on tethered balloons and hot air balloons followed by flights on both the troposphere and the stratosphere to explore different dimensions on the measurement challenge. There is now tremendous potential for information exchange and collaboration between the JPL/ISAE group, whose primary interest is planetary research, with other groups who are embarking on balloon infrasound work from a terrestrial perspective.

4.7 Conclusions

Geoacoustic investigations of the free atmosphere have begun again after a 50-year pause. Preliminary results suggest that these free flying systems have lower noise and a greater detection range. In addition, they may record elements of an acoustic wave field that seldom reaches Earth's surface. Since the stations constantly move and signal direction of arrival is difficult to ascertain, these free flying systems are not a substitute for ground arrays except in regions such as the open ocean. Rather, they compliment the existing ground infrasound network by providing a new window into geoacoustic phenomena. Continued refinement of flight systems, sensors, and experiment design will bring new discoveries and opportunities in the emerging science of high altitude geoacoustics.

Acknowledgements Sandia National Laboratories is a multi-mission laboratory managed and operated by National Technology and Engineering Solutions of Sandia, LLC., a wholly owned subsidiary of Honeywell International, Inc., for the U.S. Department of Energy's National Nuclear Security Administration under contract DE-NA0003525. The views expressed here do not necessarily reflect the views of the United States Government, the United States Department of Energy, or Sandia National Laboratories.

References

- Ames Research Staff (1953) Equations, tables, and charts for compressible flow. Technical report, National advisory committee for aeronautics. Report 1135
- Anderson JF, Johnson JB, Arechiga R, Thomas R (2014) Mapping thunder sources by inverting acoustic and electromagnetic observations. *J Geophys Res Atmos* 119:13287–13304
- Anderson JF., Johnson JB, Bowman DC, Ronan TJ (2018) The Gem infrasound logger and custom-built instrumentation. *Seismol Res Lett* 89(1):153–164
- Anderson WJ, Taback I (1991) Oscillation of high altitude balloons. *J Aircr* 28(9):606–608
- Ando H, Imamura T, Tsuda T, Tellman S, Pätzold M, Häusler B (2015) Vertical wavenumber spectra of gravity waves in the Venus atmosphere obtained from Venus express radio occultation data: evidence for saturation. *J Atmos Sci* 72:2318–2329
- Balachandran NK (1983) Acoustic and electric signals from lightning. *J Geophys Res* 88(C6):3879–3884
- Banister JR, Hereford WV (1991) Observed high-altitude pressure waves from an underground and a surface explosion. *J Geophys Res* 96(D3):5185–5193
- Barat C, Cot C, Sidi C (1984) On the measurement of the turbulence dissipation rate from rising balloons. *J Atmos Ocean Technol* 1:270–275
- Barr R, Llanwyn Jones D, Rodger CJ (2000) ELF and VLF radio waves. *J Atmos Solar-Terr Phys* 62:1689–1718
- Barthol P, Gandorfer A, Solanki SK, Schüssler M, Chares B, Curdt W, Deutsch W, Feller A, Germerott D, Grauf B, Heerlein K, Hirzberger J, Kolleck M, Meller R, Muller R, Riethmüller TL, Tomasch G, Knölker M, Lites BW, Card G, Elmore D, Fox J, Lecinski, A, Nelson P, Summers R, Watt A, Martínez Pilet V, Bonet JA, Schmidt W, Berfkfeld T, Title AM, Domingo V, Gasent Blesa JL, del Toro Iniesta JC, López Jiménez A, Álvarez Herrero A, Sabau-Graziati L, Widani C, Haberler P, Härtel K, Kampf D, Levin T, P'erez Grande I, Sanz-Andrés A, Schmidt E (2011) The sunrise mission. *Solar Phys* 268:1–34
- Beech M (1998) Venus-intercepting meteoroid streams. *Mon Not R Astron Soc* 294:259–264

- Blamont J (1985) The exploration of the atmosphere of Venus by balloons. *Adv Space Res* 5(9):99–106
- Bowman DC (2016) Infrasound from ground to space. PhD thesis, The University of North Carolina at Chapel Hill
- Bowman DC, Lees JM (2015a) Infrasound in the middle stratosphere measured with a free flying acoustic array. *Geophys Res Lett* 42(22):10010–10017
- Bowman DC, Lees JM (2015b) Near real time weather and ocean model data access with rNOMADS. *Comput Geosci* 78:88–95
- Bowman DC, Lees JM (2016) Direct measurement of the acoustic wave field in the stratosphere. In: Proceedings of the 2016 IEEE aerospace conference
- Bowman DC, Norman PE, Yang X (2015) Solar balloons: a low cost, multi-hour flight system for the lower stratosphere
- Bowman JR, Baker GE, Bahavar M (2005) Ambient infrasound noise. *Geophys Res Lett* 32:L09803
- Bretherton FP (1969) Lamb waves in a nearly isothermal atmosphere. *Q J R Meteorol Soc* 95:754–757
- Brown P, Spalding RE, ReVelle DO, Tagliaferri E, Worden SP (2002a) The flux of small near-Earth objects colliding with the Earth. *Nature* 420:294–296
- Brown PG, Whitaker RW, ReVelle DO, Tagliaferri E (2002b) Multi-station infrasonic observations of two large bolides: signal interpretation and implications for monitoring of atmospheric explosions. *Geophys Res Lett* 29(13):1636
- Cahyadi, M. N. and Heki, K. (2015). Coseismic ionospheric disturbance of the large strike-slip earthquakes in North Sumatra in 2012: m_w dependence of the disturbance amplitudes. *Geophys J Int* 200:116–129
- Campus P, Christie DR (2010) Worldwide observations of infrasonic waves. In Le Pichon A, Blanc E, Hauchecorne A (eds) *Infrasound monitoring for atmospheric studies*. Springer Science and Business Media, pp 185–234
- Ceranna L, Matoza R, Hupe P, Le Pichon A, Landés M (2019) Systematic array processing of a decade of global IMS infrasound data. In: Le Pichon A, Blanc E, Hauchecorne A (eds) *Infrasound monitoring for atmospheric studies*, 2nd edn. Springer, Dordrecht, pp 471–482
- Christie DR, Campus P (2010) The IMS infrasound network: Design and establishment of infrasound stations. In Le Pichon A, Blanc E, Hauchecorne A (eds) *Infrasound monitoring for atmospheric studies*, Springer Science and Business Media, pp 29–75
- Chum J, Hruska F, Zednik J, Lastovicka J (2012) Ionospheric disturbances (infrasound waves) over the Czech Republic excited by the 2011 Tohoku earthquake. *J Geophys Res* 117:A08319
- Coffman JW (1965) A balloon-borne microphone system. In: Korn AO (ed) *Proceedings of the 1964 Air Force Cambridge research laboratories scientific balloon symposium*, L. G. Hanscom Field, Bedford, Massachusetts
- Davies K, Jones JE (1973) Acoustic waves in the ionospheric F2 region produced by severe thunderstorms. *J Atmos Terr Phys* 35:1744–1787
- Dawton DI, Elliot H (1953) Day and night measurements of the total cosmic ray intensity at balloon altitudes. *J Atmos Terr Phys* 3:217–222
- de Groot-Hedlin C, Hedlin MA (2015) A method for detecting and locating geophysical events using groups of arrays. *Geophys J Int* 203:960–971
- de Jong M (2015) Venus altitude cycling balloon. In: Venus lab and technology workshop
- Doerenbecher A, Basdevant C, Drobinski P, Durand P, Fesquet C, Bernard F, Cocquerez P, Verdier N, Vargas A (2016) Low atmosphere drifting balloons: platforms for environmental monitoring and forecast improvement. *Bull Am Meteorol Soc*
- Drobzheva YV, Krasnov VM (2003) The acoustic field in the atmosphere and ionosphere caused by a point explosion on the ground. *J Atmos Solar-Terr Phys* 65:369–377
- Edwards WN, Brown PG, ReVelle DO (2006) Estimates of meteoroid kinetic energies from observations of infrasonic airwaves. *J Atmos Solar-Terr Phys* 68:1136–1160
- Farges T, Blanc E (2010) Characteristics of infrasound from lightning and sprites near thunderstorm areas. *J Geophys Res Space Phys* 115:A00E31

- Fee D, Haney M, Matoza R, Szuberla C, Lyons J, Waythomas C (2016) Seismic envelope-based detection and location of ground-coupled airwaves from volcanoes in Alaska. *Bulletin of the Seismol Soc Am* 106(3):1024–1035
- Fee D, Matoza RS (2013) An overview of volcano infrasound: from hawaiian to plinian, local to global. *J Volcanol Geoth Res* 249:123–139
- Frankel C (1996) *Volcanoes of the solar system*. Cambridge University Press
- Fukuhara T, Futaguchi M, Hashimoto GL, Horinouchi T, Imamura T, Iwagaimi N, Koyama T, Murakami S, Nakamura M, Ogohara K, Sato M, Suzuki M, Taguchi M, Takagi S, Ueno M, Watanabe S, Yamada M, Yamazaki A (2017) Large stationary gravity wave in the atmosphere of Venus. *Nat Geosci*
- Garcia RF, Mimoun D, Brissaud Q, Poler G, Lebonnois S (2016). Infrasound from Venus quakes: numerical modeling and balloon observation project. In: International Venus conference
- Green DN, Bowers D (2010) Estimating the detection capability of the international monitoring system infrasound network. *J Geophys Res* 115:D18116
- Guzik TG, Besse S, Calongne A, Dominique A, Ellison SB, Gould R, Granger D, Olano D, Smith D, Stewart M, Wefel JP (2008) Development of the High Altitude Student Platform. *Adv Sp Res* 42:1704–1714
- Haack A, Gerding M, Lübken F-J (2014) Characteristics of stratospheric turbulent layers measured by LITOS and their relation to the Richardson number. *J Geophys Res Atmos* 119:10605–10618
- Herrin ET, Kim TS, Stump B (2006) Evidence for an infrasound waveguide. *Geophys Res Lett* 33:L07815
- Hickey MP, Schubert G, Walterscheid RL (2001) Acoustic wave heating of the thermosphere. *J Geophys Res Sp Phys* 106(A10):21543–21548
- Jet propulsion laboratory (2016) Fireball and bolide reports
- Jones JS (1995) Reversible fluid balloon altitude control concepts. In: Proceedings of the 11th lighter-than-air systems technology conference
- Krasnov VM, Drobzheva YV, Chum J (2015) Far-field coseismic ionospheric disturbances of Tohoku earthquake. *J Atmos Solar-Terr Phys* 135:12–21
- Krasnov VM, Drobzheva YV, Lastovicka J (2007) Acoustic energy transfer to the upper atmosphere from sinusoidal sources and a role of nonlinear processes. *J Atmos Solar-Terr Phys* 69:1357–1365
- Lally VE (1967) Superpressure balloons for horizontal soundings of the atmosphere. Technical report, National Center for Atmospheric Research
- Lally VE (1991) Manned orbital balloon flight—available techniques. In: International balloon technology conference
- Landès M, Ceranna L, Le Pichon A, Matoza RS (2012) Localization of microbarom sources using the IMS infrasound network. *J Geophys Res* 117:D06102
- Le Pichon A, Ceranna L, Pilger C, Mialle P, Brown D, Herry P, Brachet N (2013) The 2013 Russian fireball largest ever detected by CTBTO infrasound sensors. *Geophys Res Lett* 40:3732–3737
- Le Pichon A, Ceranna L, Vergoz J (2012) Incorporating numerical modeling into estimates of the detection capability of the IMS infrasound network. *J Geophys Res* 117:D05121
- Le Pichon A, Herry P, Mialle P, Vergoz J, Brachet N, Garcés M, Drob D, Ceranna L (2005) Infrasound associated with the 2004–2005 large Sumatra earthquake and tsunami. *Geophys Res Lett* 32:L19802
- Lighthill J (1978) *Waves in fluids*. Cambridge University Press, Cambridge, England
- Lognonné P, Banerdt WB, Hurst K, Mimoun D, Garcia R, Lefeuvre M, Gagnepain-Beyneix J, Wiczorek M, Mocquet A, Panning M, Beucler E, Deraucourt S, Giardini D, Boschi L, Christensen U, Goetz W, Pike T, Johnson C, Weber R, Larmat K, Kobayashi N, Tromp J (2012). InSight and single-station broadband seismology: From signal and noise to interior structure determination. In: 43rd lunar and planetary conference
- Mabie J, Bullett T, Moore P, Vieira G (2016) Identification of rocket-induced acoustic waves in the ionosphere. *Geophys Res Lett*

- Marcillo O, Johnson JB, Hart D (2012) Implementation, characterization, and evaluation of an inexpensive low-power low-noise infrasound sensor based on a micromachined differential pressure transducer and a mechanical filter. *J Atmos Ocean Technol* 29:1275–1284
- Marcq E, Bertaux J-L, Montmessin F, Belyaev D (2013) Variations of sulphur dioxide at the cloud top of Venus's dynamic atmosphere. *Nat Geosci* 6:25–28
- Marty J (2019) The IMS infrasound network: current status and technological developments. In: Le Pichon A, Blanc E, Hauchecorne A (eds) *Infrasound monitoring for atmospheric studies*, 2nd edn. Springer, Dordrecht, pp 3–62
- Matoza RS, Green DN, Le Pichon A, Shearer PM, Fee D, Mialle P, Ceranna L (2017) Automated detection and cataloging of global explosive volcanism using the International Monitoring System infrasound network. *J Geophys Res Sol Earth* 122:2946–2971
- Matoza RS, Landés M, Le Pichon A, Ceranna L, Brown D (2013) Coherent ambient infrasound recorded by the International Monitoring System. *Geophys Res Lett* 40:429–433
- Meecham WC, and Wescott, J. W. (1965). High-altitude noise background. In: *Proceedings of the 5th international congress on acoustics*
- Mentik JH, Evers LG (2011) Frequency response and design parameters for differential microbarometers. *J Acoust Soc Am* 130(1):33–41
- Morris AL (ed) (1975) *Scientific ballooning handbook*. National Center for Atmospheric Research. NCAR-TN/1A-99
- Mutschlechner JP, Whitaker RW (1997) *The design and operation of infrasonic microphones*. Technical report, Los Alamos National Laboratories
- Naka Y, Shindo S, Makino Y, Kawakami H (2013) *Systems and methods for aerial and ground-based sonic boom measurement*. Technical report, Japan Aerospace Exploration Agency
- Negraru PT, Golden P, Herrin ET (2010) Infrasound propagation in the “Zone of Silence”. *Seismo Res Lett* 81(4):615–625
- Negraru PT, Herrin ET (2009) On infrasound waveguides and dispersion. *Seismo Res Lett* 80(4):565–571
- NOAA (1976) *U.S. standard atmosphere 1976*. Technical report, National Oceanic and Atmospheric Administration, National Aeronautics and Space Administration, and the United States Air Force
- Officer CB (1958) *Introduction to the theory of sound transmission*. McGraw Hill Book Company
- Peebles C (1997) *High frontier: The U. government printing office, S. Air Force and the Military Space Program*. The U. S. Government Printing Office, U. S
- Pilger C, Bittner M (2009) Infrasound from tropospheric sources: impact on mesopause temperature? *J Atmos Solar-Terr Phys* 71:816–822
- Quinn EP, Holzworth RH (1987) Quasi-lagrangian measurements of density surface fluctuations and power spectra in the stratosphere. *J Geophys Res* 92(D9):10926–10932
- Raspet R, Abbott J-P, Webster J, Yu J, Talmadge C, Alberts II K, Collier S, Noble J (2019) New systems for wind noise reduction for infrasonic measurements. In: Le Pichon A, Blanc E, Hauchecorne A (eds) *Infrasound monitoring for atmospheric studies*, 2nd edn. Springer, Dordrecht, pp 91–124
- Rayleigh (1894) *The theory of sound*, vol 2. Macmillan and Co
- Rind D (1977) Heating of the lower thermosphere by the dissipation of acoustic waves. *J Atmos Terr Phys* 39:445–456
- Rind D (1978) Investigation of the lower thermosphere results of ten years of continuous observations with natural infrasound. *J Atmos Terr Phys* 40:1199–1209
- Russell CT, Zhang TL, Delva M, Magnes W, Strangeway RJ, Wei HY (2007) Lightning on Venus inferred from whistler-mode waves in the ionosphere. *Nature* 450:661–662
- Sagdeev RS, Linkin VM, Blamont JT, Preston RA (1986) The VEGA Venus balloon experiment. *Science* 231(4744):1407–1408
- Saito, Y. (2014). *Quest for altitude*. Accessed 2 Dec 2016
- Shalygin EV, Markiewicz WJ, Basilevsky AT, Titov DV, Ignatiev NI, Head JW (2015) Active volcanism on Venus in the Ganiki Chasma rift zone. *Geophys Res Lett* 42:4762–4769

- Smrekar SE, Stofan ER, Mueller N, Treiman A, Elkins-Tanton L, Helbert J, Piccioni G, Drossart P (2010) Recent hot-spot volcanism on Venus from VIRTIS emissivity data. *Science* 328:605–608
- Squyres S (2011) Vision and voyages for planetary science in the decade 2013–2022
- Stevenson D, Cutts J, Mimoun D (2015) Probing the interior structure of Venus. Technical report, Keck Institute for Space Studies
- Tailpied D, Le Pichon A, Marchetti E, Assink J, Vergniolle S (2016) Assessing and optimizing the performance of infrasound networks to monitor volcanic eruptions. *Geophys J Int*
- Veggeberg K (2012) Development of a sonic boom measurement system at JAXA. In: Proceedings of the acoustics 2012 Nantes conference
- Volcano World (2017) Volcano world: Venus. Accessed 4 Jan 2017
- Walker KT, Hedlin MA (2010) A review of wind-noise reduction technologies. In: *Infrasound monitoring for atmospheric studies*, chapter 5, pp 141–182. Springer Science and Business Media
- Walterscheid RL, Hickey MP (2005) Acoustic waves generated by gusty flow over hilly terrain. *J Geophys Res Sp Phys* 110:A10307
- Waxler R, Gilbert KE (2006) The radiation of atmospheric microbaroms by ocean waves. *J Acoust Soc Am* 119(5):2651–2664
- Weaver RL, McAndrew J (1995) The Roswell report: fact versus fiction in the New Mexico desert. Government Printing Office, U.S
- Wescott JW (1961) Atmospheric background at high altitudes. In: Proceedings of the symposium on atmospheric acoustic propagation
- Wescott JW (1964a) Acoustic detection of high-altitude turbulence. Technical report, The University of Michigan
- Wescott JW (1964b) Acoustic detection of high altitude turbulence. In: Korn AO (ed) Proceedings of the 1964 Air Force Cambridge Research Laboratories scientific ballooning symposium, L. G. Hanscom Field, Bedford, Massachusetts
- Wu Y, Llewellyn Smith SG, Rottman JW, Broutman D, Minister J-BH (2016) The propagation of tsunami-generated acoustic-gravity waves in the atmosphere. *J Atmos Sci* 73:3025–3036
- Yajima N, Izutsu N, Imamura T, Abe T (2009) *Scientific Ballooning: Technology and applications of exploration balloons floating in the stratosphere and the atmospheres of other planets*. Springer Science and Business Media
- Young EF, Brown P, Boslough M, Ballard C, Dougherty E, Dullea C, Garner K, Heaney M, Thom I., Von Hendy, M., Wahl, K., and Young, E. (2016). Detection of infrasound disturbances from the Earth’s stratosphere. In: Proceedings of the 2016 IEEE aerospace conference
- Zhang SD, Yi F, Huang CM, Huang KM (2012) High vertical resolution analyses of gravity waves and turbulence at a midlatitude station. *J Geophys Res Atmos* 117:D02103